Spatial characteristics of thin scattering layers observed by airborne LIDAR

James H. Churnside
NOAA Earth System Research Laboratory
325 Broadway
Boulder, CO 80305
james.h.churnside@noaa.gov

Abstract: Existing airborne LIDAR data were examined for the presence of thin (< 3 m) optical scattering layers for several regions of the ocean. The data were collected during late spring and summer during the period between 1997 and 2003. The regions covered were coastal waters near the west coast of North America, the north and west coasts of the Iberian Peninsula, and the west coast of Norway. Over 2000 km of thin layers were identified in about 80000 km of flight tracks. Thin layers were most prevalent where there was a large freshwater discharge into the ocean. Thin layers were also observed within warm-core eddies in the Gulf of Alaska. Thin layers were practically nonexistent during strong upwelling events. Thin layers demonstrated complex spatial structure, including multiple layers and perturbations by internal waves. The depths of thin layers were only weakly correlated with mixed layer depth inferred from CTD measurements because of the spatial and temporal variability in thin layer depth.

1. Introduction

The development of instruments capable of measuring the distribution of plankton with high vertical resolution led to the discovery of thin, coherent layers in the ocean (Pieper and Holliday, 1984; Holliday, et al, 1998; 2003). These layers range between about 10 cm and a few m thick. They can extend for kilometers, persist for days, and contain plankton concentrations many times that of the surrounding water. This concentration affects the chemical (Hanson and Donaghay, 2001) and biological (Cowles, et al, 1998) dynamics of the pelagic zone. It also affects the acoustic and optical (Petrenko, et al, 1998; Zaneveld and Pegau, 1998) properties of the water column.

Much of the detailed information about thin layers comes from intensive studies in 1996 (Dekshenieks et al, 2001; Alldredge, et al, 2002) and 1998 (McManus, et al, 2003) in a shallow fjord in the northwestern United States. In the first of these studies, thin layers were observed in 54% of the 120 measurement stations. Thickness ranged between 0.12 and 3.6 m, with 80% < 2 m thick. Most occurred near the surface; 80% were < 10m depth. Most (71%) were within the pycnocline or at its base.

The large scale of these layers, coupled with the typically shallow depth, suggests airborne lidar as a technique to investigate their spatial characteristics. Oceanographic lidars use visible light, generally green, to investigate the upper ocean. Since it is visible light, it scatters from everything in the water column from water molecules to the largest submarines, and including phytoplankton and zooplankton. Hoge, et al (1988) reported airborne lidar observations of scattering layers in the NW Atlantic. Vasilkov, et al (2001) observed layers in the same area using a polarized lidar. Churnside and Ostrovsky (2004) reported observations of a strong internal wave in the Gulf of Alaska by the perturbations of a scattering layer. However, none of these investigations were interested in the layer thickness.

NOAA is developing an airborne LIDAR system for surveys of epipelagic fish (Churnside, et al, 2001), and has performed a number of experimental surveys in regions where stratification of the water column might be expected. The first flight tests of the system were over the Southern California Bight between 30 March and 21 April, 1997 (Churnside, et al, 2001). Subsequent tests were made over the NW Atlantic along the coast of the Iberian Peninsula between 22 August and 9 September, 1998, over the Gulf of Alaska between 20 July and 10 September, 2001 and between 11 May and 1 September, 2002, over the Norwegian Sea between 15 and 23 July, 2002, over the NE Pacific along the coast of Oregon and Washington between 9 and 17 July, 2003, and over the Gulf of Alaska again between 20 July and 2 August, 2003. These data were examined for the presence of thin layers, where we have used "less than 3 m" as our definition of thin. Data collected during the winter (e.g., Churnside, et al, 2003) were not included in this study.

Because of the fisheries application, the surveys were generally done in areas where upwelling brings nutrients to the surface to support high productivity. Upwelling can have several effects relevant to the formation of thin layers. It can bring nutrients to

the surface, allowing plankton growth. It can increase the overlying density gradient, producing thinner layers. However, the strong winds that can create upwelling can also destroy density gradients on which layers might form, at least near the surface. We see evidence for all of these effects in the LIDAR data.

Thin layers show up very clearly in a lidar signal (Figure 1). The layer in this case was at a depth of 12 - 15 m. The thickness varied from less than 1 m to about 5 m, with the thickest part at the right end. Figure 2 presents a typical profile through the thinner part of the layer at a distance of about 500 m from the start of Figure 1. The figure shows both the raw LIDAR return and the return after processing to remove the effects of the uniform background scattering level and to correct for the attenuation of light in the water. The depth of the peak is at about 12.3 m, and the full width at half maximum is about 2.7 m. After deconvolution with the pulse shape, as discussed in the next section, the estimated layer thickness is 2.5 m. The peak volume backscatter coefficient for this profile was 2.6×10^{-6} $m^{-1}sr^{-1}$, compared with a maximum value of 3.9×10^{-6} $m^{-1}sr^{-1}$ for the whole layer.

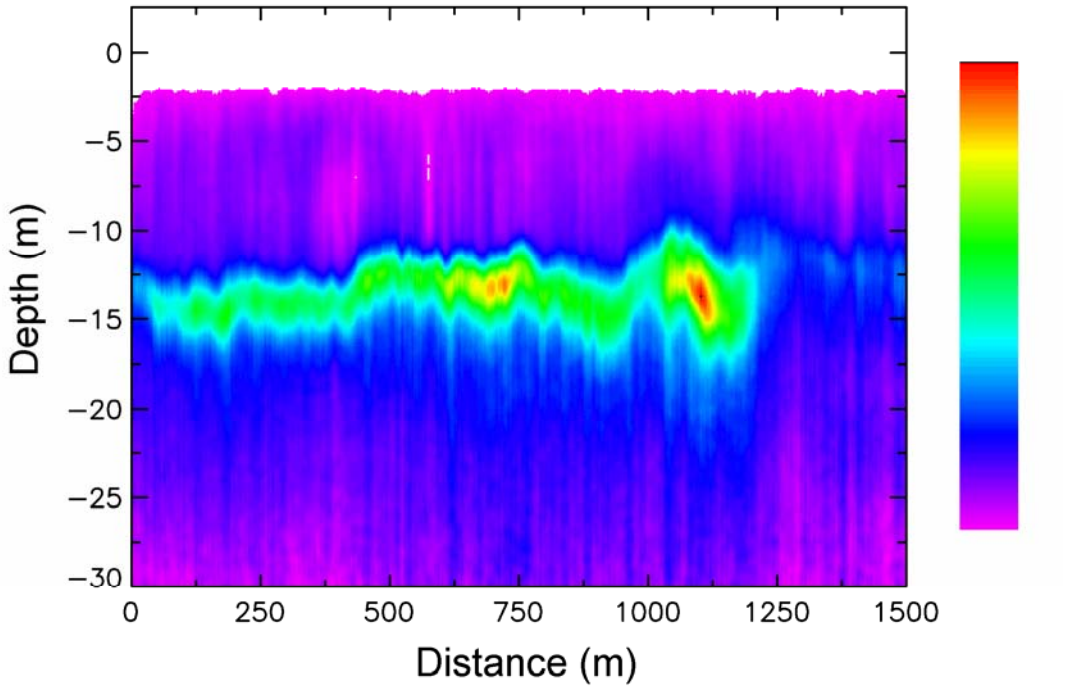

Fig. 1. Vertical slice of a typical plankton layer as seen by the LIDAR. The relative color scale is shown to the right, with the maximum value representing a volume backscatter coefficient of 3.9×10^{-6} $m^{-1}sr^{-1}$.

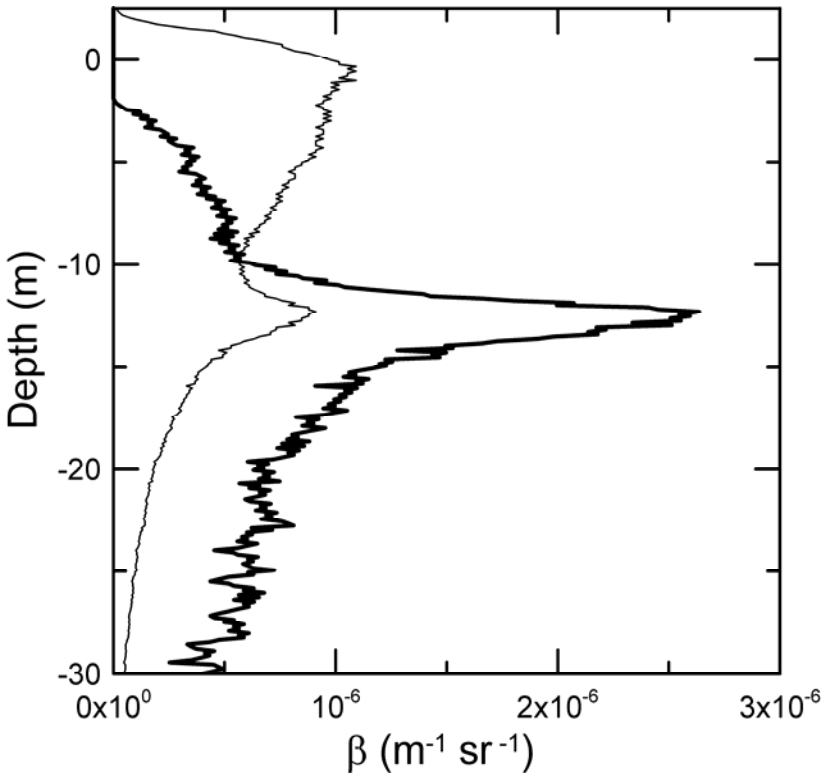

Fig. 2. Single depth profile of volume backscatter coefficient β from the slice of Fig. 1. The thin line is the raw LIDAR return and the heavy line is the return after processing to remove the effects of the uniform background scattering level and to correct for the attenuation of light in the water.

2. Materials and Methods

The NOAA Fish LIDAR is a non-scanning, profiling system (Churnside et al, 2001). It transmits about 100 mJ of linearly polarized green (532 nm) light in a 12 ns pulse at a rate of 30 pulses per second. It is generally pointed about 15º off nadir to minimize the specular reflection from the sea surface. The diameter of the laser spot on the surface is generally 5 m for daytime flights and 15 m for nighttime flights. The 5 m spot is large enough that the power density at the surface is safe for humans (ANSI, 1993) and marine mammals (Zorn, et al, 2000) at the surface. At the same time, it is small enough that the background sunlight is a small part of the overall signal. At night, background sunlight is not present, and the spot is expanded to reduce the attenuation (Gordon, 1982). The scattered light from the water column is collected by a telescope, detected by a photomultiplier tube, logarithmically amplified to increase the dynamic range, and digitized at a rate of 10^9 samples per second. Generally, the receiver is configured to detect linearly polarized light orthogonal to the transmitter to increase detectability (Lewis, et al, 1999).

The raw data from the LIDAR were stored on disk for later processing. Aircraft position from GPS and time were recorded in the same data files. Each file contains the data from 2000 LIDAR pulses, which corresponds to just over 1 minute of data. This allows the data files to be uniquely named by the day, hour, and minute at which each

was created. The data format is a standard 8-bit image format, where rows and columns present different samples within a pulse and different pulses, respectively. This allows the raw data files to be viewed with standard image processing software.

The depth resolution limit set by the sample rate is about 11 cm, which is a good match to the thinnest layers of interest. However, this resolution is degraded by the effects of the laser pulse, which illuminates a slice of the water column about 1.3 m thick at any instant. The shape of the illumination profile can be approximated by $z \exp(-1.8z)$, as illustrated in Figure 3. The sample points in the figure show that the pulse is sampled at a rate much greater than its width. The shape of the LIDAR signal received from a layer is the convolution of the pulse shape with the profile of the scattering strength through the layer. The figure illustrates the resulting pulse shape for a uniform layer that is 1 m (9 samples) thick. The thickness of the composite pulse is about 1.7 m. Note, too, the delay to the peak of the convolved pulse. The actual difference should be half or the layer thickness, or 0.5 m. The actual delay in the figure is about 0.65 m, so there is a small error in the estimate of the depth of very thin layers. As the layer thickness increases, this error gets smaller, and we will neglect it throughout.

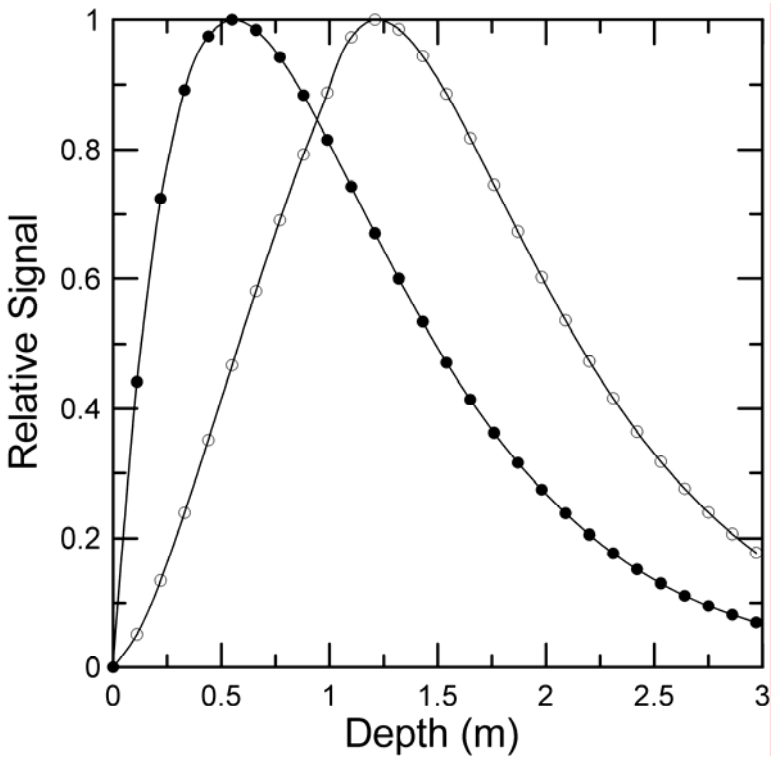

Fig. 3. Approximate profile of the raw laser pulse (solid circles) and the pulse convolved with a uniform layer with a thickness of 1 m (open circles).

Because the return is a convolution, we can get an estimate of the layer profile by a deconvolution. This implies that we can estimate the layer thickness by the square root of the difference between the squares of the measured thickness and 1.3 m. This works fairly well for layers thicker than the pulse length; the uncertainty in the estimated layer thickness is about 24 cm for an actual thickness of 3 m and an uncertainty of 1 sample

(11 cm) in the measured thickness. For thinner layers, the uncertainty is greater: 36 cm for a 1 m thick layer and 50 cm for a 0.7 m thick layer.

The first step in the data analysis was a visual inspection of the original data files, which contain the logarithm of the raw LIDAR data. A list was made of those files that contained visible layers of any thickness, and these were subjected to further processing according to the following steps:

a. The signal from ambient light was estimated by the average of the last 100 samples of each pulse, which was after the returned laser light had decayed to negligible levels. Since the ambient light adds linearly to the laser signal, the estimated value was subtracted from each sample in the LIDAR return.

b. A correction was applied for the range-squared geometric loss.

c. The background scattering level and exponential attenuation were estimated using the signal from a depth of 2 m and the signal from a depth of 0.8 times the maximum penetration depth. The maximum penetration depth was defined as the depth at which the signal fell below a value that was 10 standard deviations of the noise above the ambient light level. The upper value of 2 m was chosen to avoid the signal from breaking waves and foam that occurs in some of the near-surface data. This signal can extend to an apparent depth as great as 2 m under high wind conditions, which probably corresponds to the depths of the troughs.

d. The exponentially decaying background signal was subtracted from each profile, and the result was corrected for the measured attenuation. Localized regions of enhanced scattering were identified where the full width at half maximum was less than 3 m; regions thicker than 3 m were not considered to be thin for the purpose of this study. The result of this step is the processed data as shown, for example, by the heavy line in Figure 2.

e. The image of each original data file was displayed on a computer screen with the positions of the peaks of the localized regions of enhanced backscatter that were identified in Step 4 superimposed (Fig. 4). Each image corresponds to 4 – 6 km along the flight track, depending on aircraft speed. Coherent layers were identified as regions where the individual peak positions were tightly clustered. Finally, the length, average depth, average thickness, and standard deviation of thickness were calculated for each layer.

Selection of layers was somewhat subjective. As an example, 2 layers were selected from the data presented in Fig. 4. The first extends from 1660 m to 2590 m, and the second from 3660 m to 5210 m, both near 5 m in depth. Other peaks that can be seen in the figure were not selected, because they were too scattered. In many cases, what we identified as thin layers were thin regions of much larger layers. Often, there were gaps within the identified layers. In Figure 4, two gaps can be seen in each of the two layers, and we might have considered each of these layers to be 3 separate layers. If we denote the layers by 1 on the left and 2 on the right, and the sublayers within each of these layers by *a* – *c* from left to right, we can look at the differences that might be introduced by how we selected these layers. This case was chosen because the gaps were about the largest that were allowed within a single layer. The statistics for the 2 layers, the 6 sublayers, and the aggregate of the sublayers for each layer are summarized in Table 1. While the

total length is about 19 % less for the total of the sublayers than for the sum of the 2 layers, the depths and thicknesses are nearly the same.

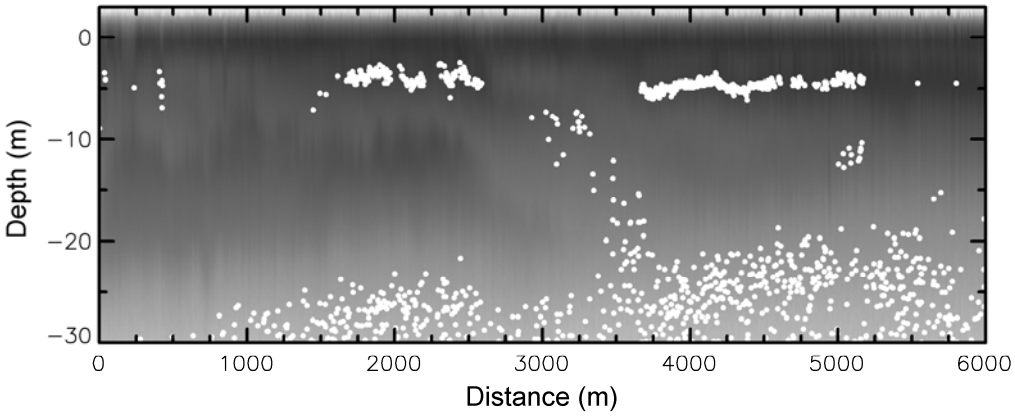

Fig. 4. Vertical slice of raw lidar data along 6 km of flight track. Darker shading corresponds to greater lidar return on a logarithmic scale, although the gray-scale variations are difficult to see in the image. White circles mark peaks that are with full width at half maximum in depth of less than 3 m. Note the line of circles between 1660 m and 2590 m with gaps at 2000 m and 2250 m and another line between 3660 m and 5210 m with gaps at 4670 m and 4810 m.

Table 1. Comparison of results for 2 layers (denoted 1 and 2) when identified as single layers and when identified as 3 individual layers a, b, and c.

Layer	Length (m)	Depth (m)	Thickness (m)
1	930	3.92	1.77
2	1524	4.69	2.59
1a	318	3.76	1.69
1b	168	4.37	0.86
1c	294	3.95	2.36
2a	954	4.79	2.30
2b	96	4.45	2.95
2c	156	4.12	2.64
1a – 1c	780	3.96	1.76
2a – 2c	1206	4.68	2.40

The processing techniques were tested using data from a daytime flight off the west coast of Florida, where the bottom is relatively flat and homogeneous. We selected 32 segments of the bottom return with lengths from 246 m to 594 m, with an average length of 392 m. Segment depth ranged from 6.3 m to 21 m, with an average of 10.8 m. The measured thickness varied from 0.5 m to 2.5 m, with an average value of 1.8 m. Water clarity was also different from segment to segment; the attenuation coefficient ranged from 0.03 m^{-1} sr^{-1} to 0.26 m^{-1} sr^{-1}, with an average value of 0.18 m^{-1} sr^{-1}.

There are several reasons why the measured thickness of the bottom is not zero. One is the beam geometry. We are illuminating the bottom with a beam that is 5 m in diameter at an angle of about 11° (15° in air). This means that one edge of the beam will hit the bottom about 4 ns before the other, and we interpret that spread in time as a finite thickness. For an infinitesimally short laser pulse, that thickness would appear to be about 0.97 m. We modeled the combined effects of beam geometry and a Gaussian pulse with the same width as our actual pulse and got an apparent thickness of 1.5 m. After performing the deconvolution, the measured thickness would be about 0.7 m. The same model predicts that the measured thickness for our typical nighttime geometry (15 m spot) would be about 2.5 m. Of course, this effect would be larger or smaller if the bottom were sloped to create a larger or smaller angle between it and the beam. As an example, the average observed value of 1.8 m would be expected for a bottom slope of about 11° in the same plane as the incident beam or 21° in the orthogonal plane.

Another reason is roughness of the bottom, the surface, or both. Roughness on scales smaller than our beam directly spreads the return over a longer time and increases the measured thickness. For the case of bottom roughness, the height variations are added directly. For the case of surface roughness, it is the differences in optical path length that are important. This is given by the $(n - 1)$ times the physical height difference, where n is the index of refraction of sea water. To illustrate, we assume a Gaussian model of roughness and a level bottom. The observed average value of 1.8 m would be obtained for a bottom roughness with a standard deviation of about 0.3 m or a surface roughness with a standard deviation of about 1 m.

Finally, the effects of multiple scattering can increase the optical path length through the water, making the bottom appear thicker. However, this effect is probably relatively small. To estimate the magnitude of the effect, we use the Petzold results as reproduced in Mobley (1994) for the coastal ocean. The diffuse attenuation coefficient measured at 514 nm is 0.18 m^{-1} sr^{-1}, the same as our measured attenuation coefficient. The corresponding scattering coefficient is 0.219 m^{-1} and the median scattering angle is 2.53°. Thus, the excess path length at the median scattering angle would be about 4.5 mm per scattering event. To get the increase of 0.3 m that matches our observations, we would need about 4400 independent scattering events during the round trip propagation of the beam through the water, or a water depth of about 10 km.

3. Results

3.1. NE Pacific Ocean, 2003

The study region in which thin layers were most extensive was the NE Pacific Ocean along the coast of Oregon and Washington (Figure 5), and these data will be described first. The 5 long transects were flown out and back during daylight and again after dark on July 9 (44 N), 10 (45 N), 11 (46 N), 13 (47 N) and 16 (48 N). The period prior to these flights was characterized by strong upwelling, with average values for the first 7 days in July of 76 m^3s^{-1} per 100 m of coastline at 45 N and 34 m^3s^{-1} per 100 m of coastline at 48 N

(http://www.pfeg.noaa.gov/products/PFEL/modeled/indices/upwelling/upwelling.html). A period of small or negative upwelling indices existed during the flights. Sea-surface temperature data measured with an infrared radiometer on the aircraft showed a large (4 K) temperature difference between cold near-shore water and warmer water off shore along 44 N. No such pattern was observed along the other lines. Sea-surface temperature data from satellite on July 9 suggest that this pattern was in place on that date, and not an effect of warming of the near-shore water over the time period of the flights.

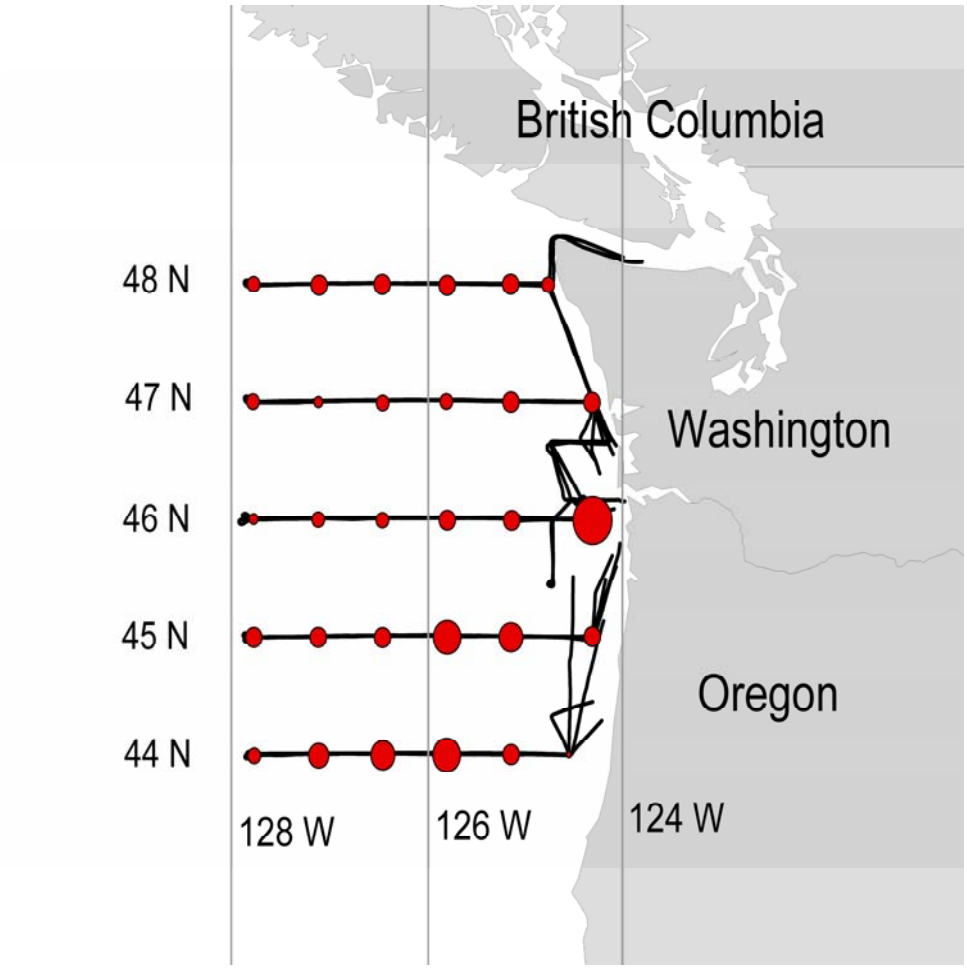

Fig. 5 Flight tracks along constant latitude lines. Red circles show relative freshness (33 ppt – surface salinity) at the CTD positions over a range of 0.07 ppt to 3.9 ppt.

The oceanography of the region is also strongly influenced by fresh water input, as can be seen in Figure 5. The plume from the Columbia River (the border between Oregon and Washington) extends from the mouth of the river southwest through the study area. Fresh water from the Strait of Juan de Fuca (between Washington and British Columbia) can be seen along the north edge of the study area. These surface salinity values correlate well ($R^2 = 0.87$) with the overall density change in the upper 50 m. The average value of this density change was quite large (1.9 kg m^3 – 1000), with a value at

the mouth of the river reaching 4.5 kg m^3 – 1000. We assume that the overall density change is related to the gradients in some sense. The CTD data available do not have the resolution to obtain reliable estimates of density gradients on the scales we would like.

In total, data were analyzed from over 8000 km of track line, about evenly divided between day and night. Thin layers were identified in just over 1000 km of those tracks, 19% of the area covered during the day and 6% at night. The average depth was 9.5 m during the day and 12.9 m at night. The average thickness was 2.2 m day or night. Multiple thin layers were not uncommon. The fraction of the layer area with multiple layers was 10.5% during the day and 2.7% at night. Even three layers were occasionally observed, (0.65% of the thin layers during the day and 0.16% at night).

Although these statistics do not include layers at the surface, layers were observed at the surface. Figure 6 presents a typical example, with dark layers right at the surface in some places, but not in others. The scale and connection with deeper layers suggests that the surface scattering layers are really the same as the deeper layers. In other data, we see a surface scattering layer that is intermittent on a scale of a few tens of meters. These are generally associated with visual observations of breaking waves, and we are confident that these are caused by scattering from breaking waves and foam. In other cases, the spatial characteristics of surface scattering are some mix of these two cases, and the source is less clear.

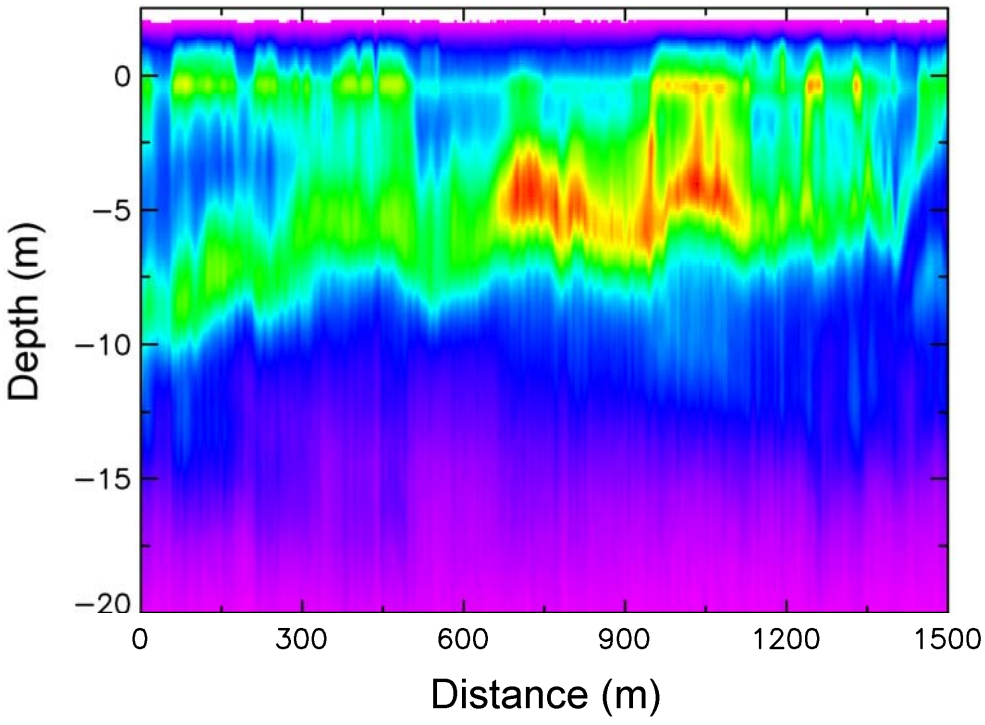

Fig. 6. Vertical slice of lidar data showing layers extending to surface.

The total coverage by thin layers observed on the outbound leg, $P(out)$, of each of the long transects in Figure 5 was well correlated with that observed on the inbound leg, $P(in)$. The values, plotted in Figure 7, have a correlation coefficient of 0.84. The linear regression is given by:

$$P(in) \quad = \quad 0.89 \pm 0.20 P(out) \quad + \quad 0.04 \pm 0.04. \tag{1}$$

This suggests that the large-scale conditions for thin layers are not changing on the 1 – 2 hour time scale of these flights.

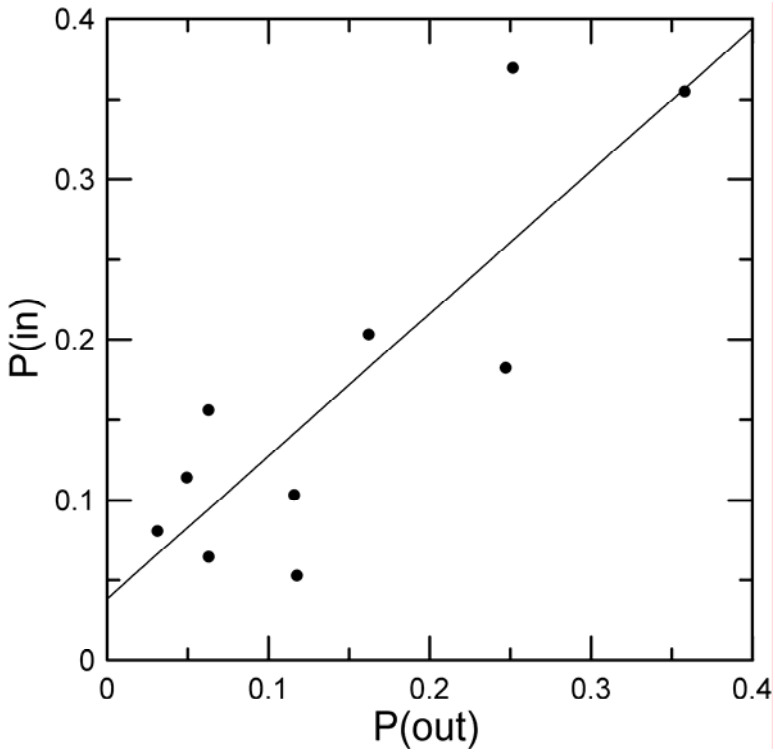

Fig. 7. Fraction of flight path covered by thin layers on the inbound leg P(in) vs that on the outbound leg, P(out), for the day and night flights each of the 5 long E-W transects.

The correlation between the day and night values (averaged over outbound and inbound legs) was even higher, 0.97. The overall values were different, however, so the slope was not nearly unity. The regression is given by:

$$P(night) \quad = \quad 0.23 \pm 0.04 P(day) \quad + \quad 0.03 \pm 0.01 \tag{2}$$

Although the layers were generally found along the same transects both day and night, far fewer were observed at night than during the day.

The observation that the average depth was greater at night than during the day is because of a greater depth penetration of the lidar during the day. The probability-density function of depth for all data (Figure 8). Both day and night, the probability density has a peak at a depth of about 4 m. When we restrict the analysis to only those layers whose volume backscatter coefficient was greater than 0.01 times the appropriate (daytime or nighttime) maximum value, that peak in the density function becomes very pronounced. This is particularly true for the daytime data, where there is a significant probability of observing a layer at a depth of around 10 m during the daytime. When we look at only the stronger layers, we see that this probability is much less, which implies that many of the layers around this depth are weakly scattering.

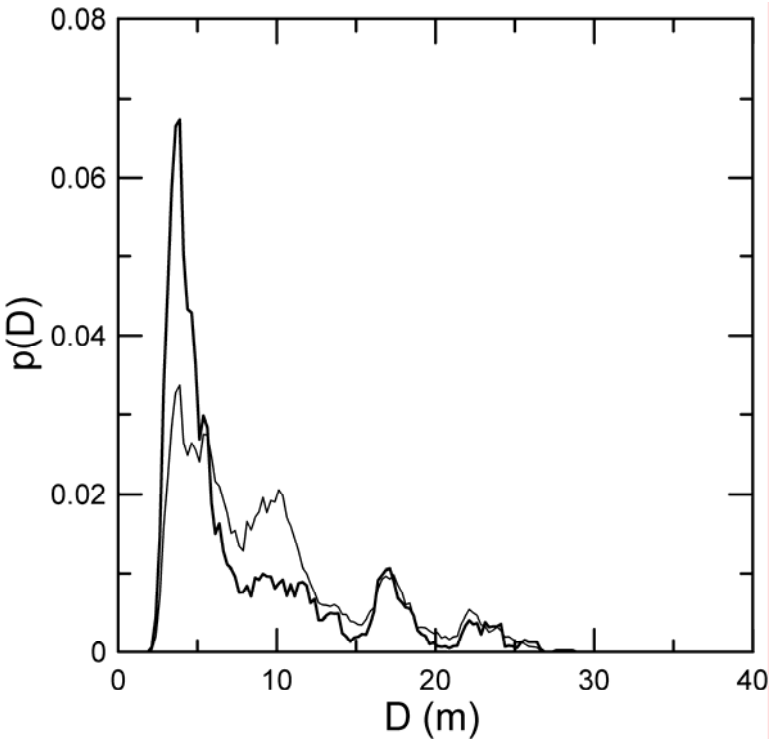

Fig. 8a. Probability density function p of depth D for all daytime layers (thin line) and those with an average volume backscatter coefficient greater than 1% of the daytime maximum value (thick line).

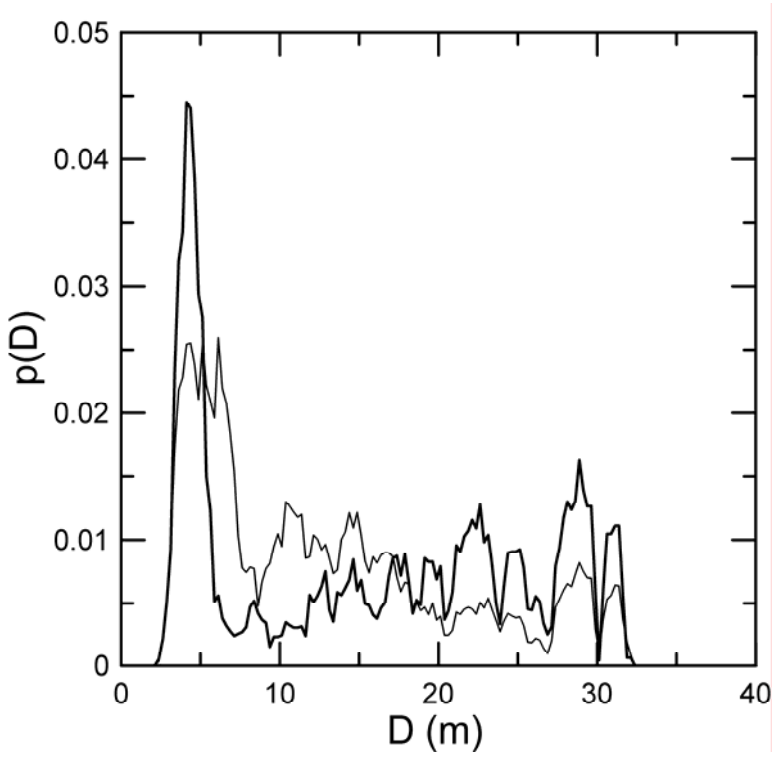

Fig. 8b. Probability density function p of depth D for all nighttime layers (thin line) and those with an average volume backscatter coefficient greater than 1% of the nighttime maximum value (thick line).

The CTD casts from the ship (Fig. 5) were made on the same day of the corresponding flight in all cases, and we can look at the distribution of the depth of thin layers around these casts. The separation of the casts along each line is about 50 km, except for the station nearest the shore. The depth of the mixed layer was estimated from profiles of the density, σ_θ, calculated from the CTD measurements. The range of values was from 4 to 26 m, with an average over the area of about 14 m. Figure 9 shows that the mixed layer was generally deeper to the north and offshore and shallower near shore and to the south.

The average depths of thin layers within 20 km of each of the CTD casts, also presented in Figure 9, show a general agreement with the mixed layer depth. The overall average of these depths was 10.8 m during the day and 13.7 m at night. The correlation between the lidar depths and the mixed layer depths was 0.66 during the day and 0.72 at night. If the values are weighted by the total length of thin layers within each region, the correlation is slightly higher, 0.74 during the day and 0.86 at night. The correlation between the daytime and nighttime lidar depths on this scale of averaging was 0.72. The worst agreement between mixed layer depth and thin layer depth was generally offshore along the 46th parallel, where the mixed depth was deeper than the thin layer depths.

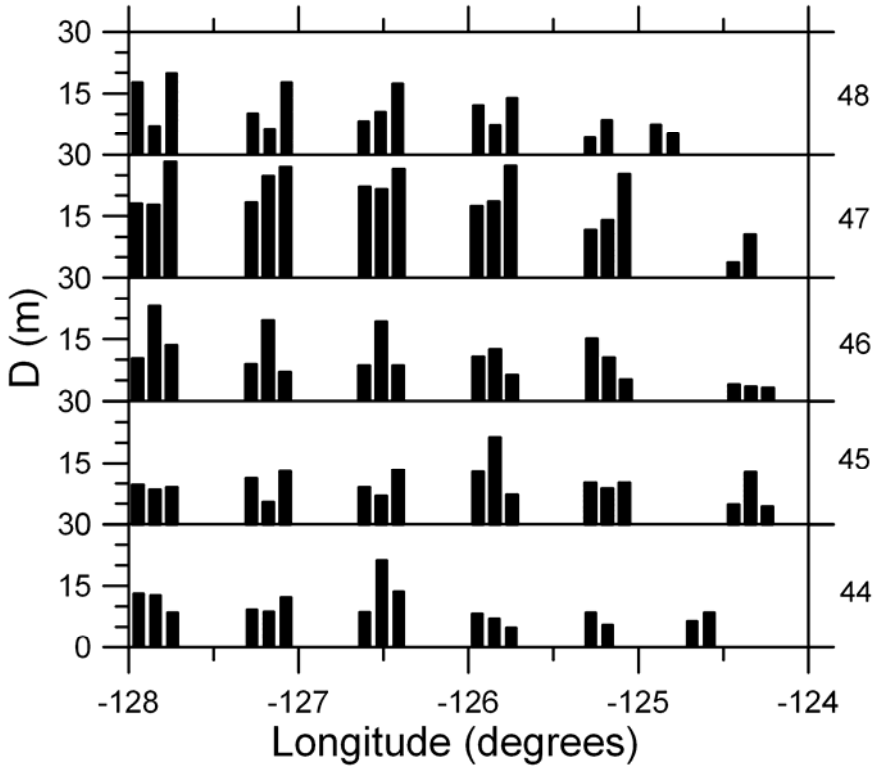

Fig. 9. Depth of mixed layer from CTD casts (center bar of 3 or right-hand bar of 2) at the longitude of the cast for each of the 5 latitude lines (labeled by latitude at the right of the plots. The bar to the left represents the average depth of thin layers within 20 km of the cast, identified by the lidar during the day. The bar to the right represents the same quantity for the night flights where thin layers were seen during the night flights.

As an example of the disagreement, we consider the conditions near the CTD cast at about 127.18 W, 46.00 N. The density profile shows a very clearly defined mixed layer down to a depth of about 20 m. No layers were seen this deep. Figure 10a shows a typical layer observed in this area during the day. While not continuous, it extends over about 1700 m at depths between 5 and 10 m. No structure is seen near a depth of 20 m, even though the daytime penetration depth in this area was about 30 m. Although a 20 km separation between CTD cast and layer was allowed in the analysis, this layer was considerably closer; the aircraft passed about 1100 m north of the cast location at a time corresponding to 1750 m in Figure 10a. These lidar data are from the outbound leg, so the layer is just north and east of the cast. Figure 10b shows a typical layer from the same area at night, and it is similar to that observed during the daytime. At night, there is a weak, thick layer just below 20 m, but this does not satisfy our criteria for a thin layer; in fact, only the shallowest segment of the upper layer, at a depth of about 5 m on the left side of the figure, qualified as a thin layer.

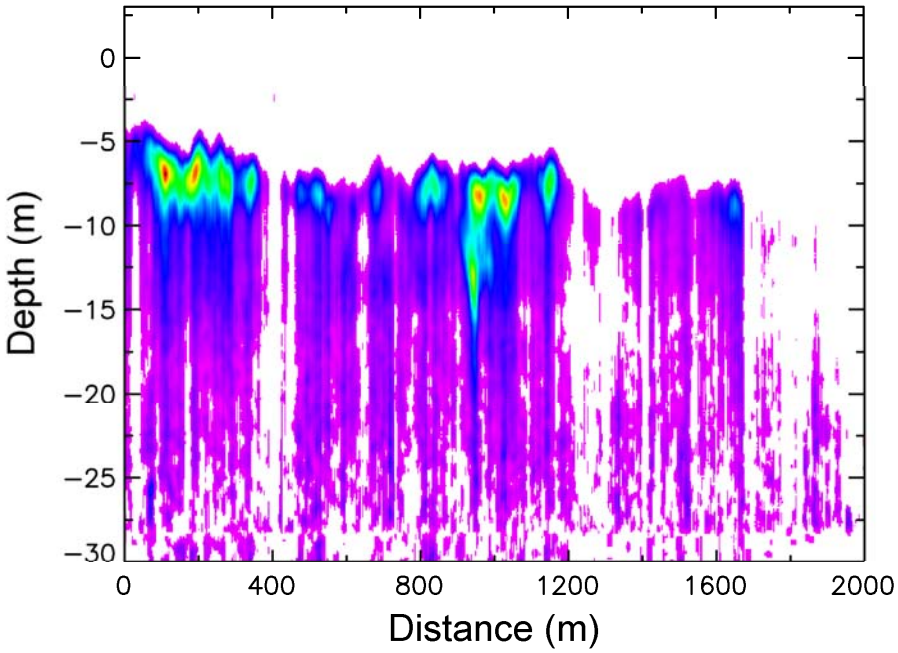

Fig. 10a. Vertical slice of lidar data from vicinity of the CTD cast considered in the text. (daytime)

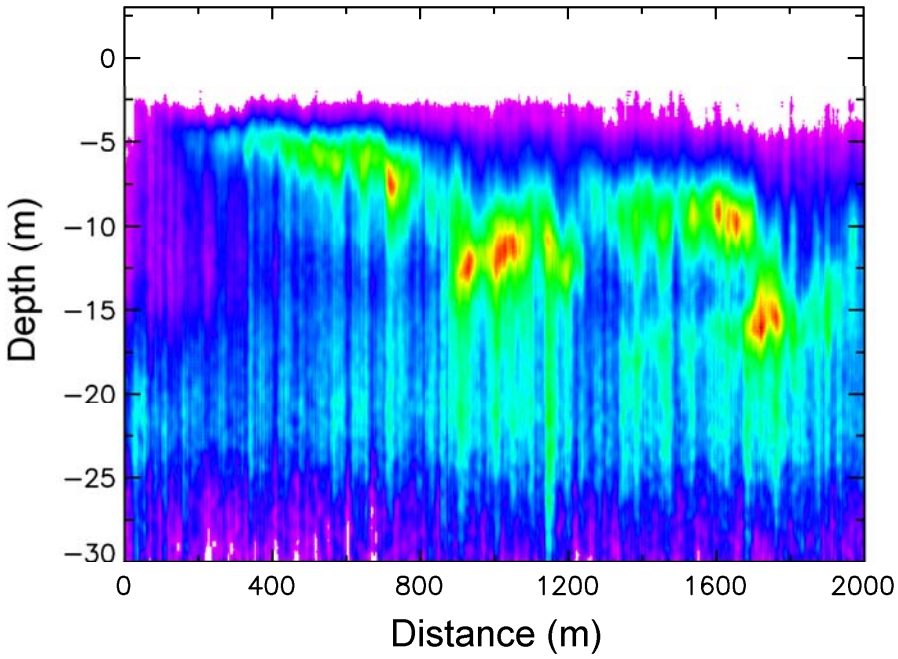

Fig. 10b. Vertical slice of lidar data from vicinity of the CTD cast considered in the text. (nighttime)

There is a moderate correlation between the average layer backscattering strength and surface salinity ($R^2 = 0.44$) and with the overall density difference between the surface and a depth of 50 m ($R^2 = 0.50$). The correlations are largely determined by the very strong layers ($\beta(\pi) = 5.7\times10^{-5}$ m^{-1} sr^{-1}) at the mouth of the Columbia River. Otherwise, the layer strengths were generally weaker to the south of the river than to the north, with the largest values (up to $\beta(\pi) = 7.1\times10^{-6}$ m^{-1} sr^{-1}) along the 48th parallel. The timing of the flights may be a factor; the flights to the south were made 2 and 3 days after the end of the upwelling event on July 7, while the flights to the north were made 6 and 9 days after the end of the event.

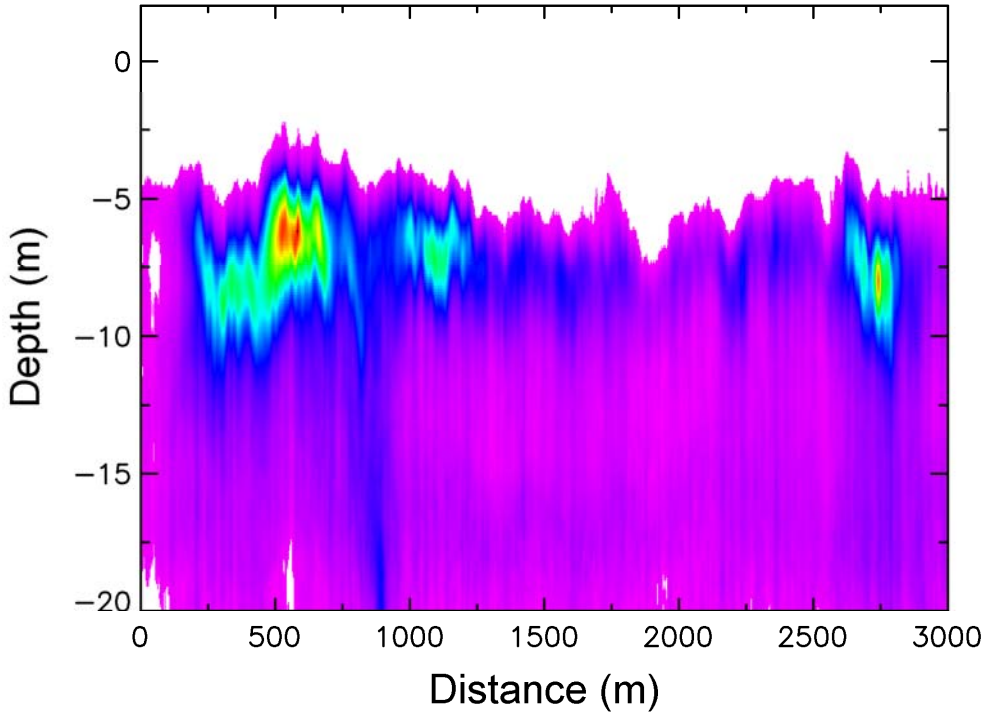

Fig. 11. Vertical slice of lidar data for long layer used in autocorrelation calculation.

The small scale characteristics of the layers vary from layer to layer, but it is instructive to consider a typical example. Figure 11 shows a layer that is about 3 km long. The average ± standard deviation of thickness for this layer was 3.00 ± 0.84 m, the depth was 7.04 ± 1.01 m, and the strength was $1.84\times10^{-7} \pm 1.51\times10^{-7}$ m^{-1} sr^{-1}. The spatial variability can best be described by the autocorrelation function, plotted in Figure 12 for each of the 3 variables. The fluctuations of layer strength have the largest scale, with an exp(-1) correlation length of about 179 m. The correlation of both thickness and depth fall off much faster, with depth changing more rapidly along the flight track than thickness. Note also the peak in the autocorrelation function of depth at a separation of about 30 m. This is probably an effect of surface waves, since we measure depth with

respect to the local surface height. Assuming that the layer itself is not affected significantly by the surface waves, the observed covariance in depth at 30 m corresponds to a surface wave with an amplitude of 0.55 m.

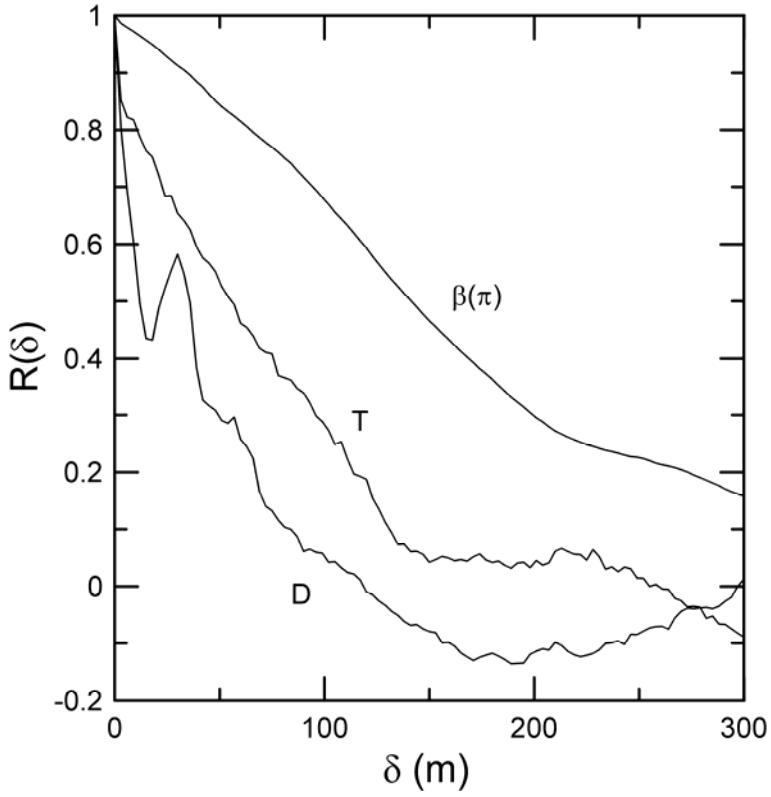

Fig. 12. Autocorrelation R as a function of spatial lag δ for strength β(π), thickness T and depth D for the layer of Fig. 11.

3.2. Gulf of Alaska, 2002

The next data set to be considered is the Gulf of Alaska, and particularly the region around Kodiak Island, Alaska. The northern Gulf of Alaska is predominately a downwelling system, but still supports a productive ecosystem (Stabeno, et al, 2004). During the time periods of the flights, there is a large fresh-water input into the eastern part of the region, which is carried westward by the Alaska Coastal Current. In the region around Kodiak Island, this current crosses several canyons in the continental shelf. The interaction of the tides and the Alaska Coastal Current with the canyons and the shallow banks between them can mix nutrients into the euphotic zone in this region.

The flight tracks (Figure 13) show a heavy concentration of the flights in the region very close to the island. In all, 19000 km were flown during daytime and 10000 km at night during two periods, May 11 – 25 and July 16 – September 1. Fewer layers were observed in this region than off the NW coast – 2.8% during the day and 0.25% at night. The average depth was less – 6.1 m day or night. The average thickness was about the same – 2.2 m day or night. Multiple thin layers were very rarely observed.

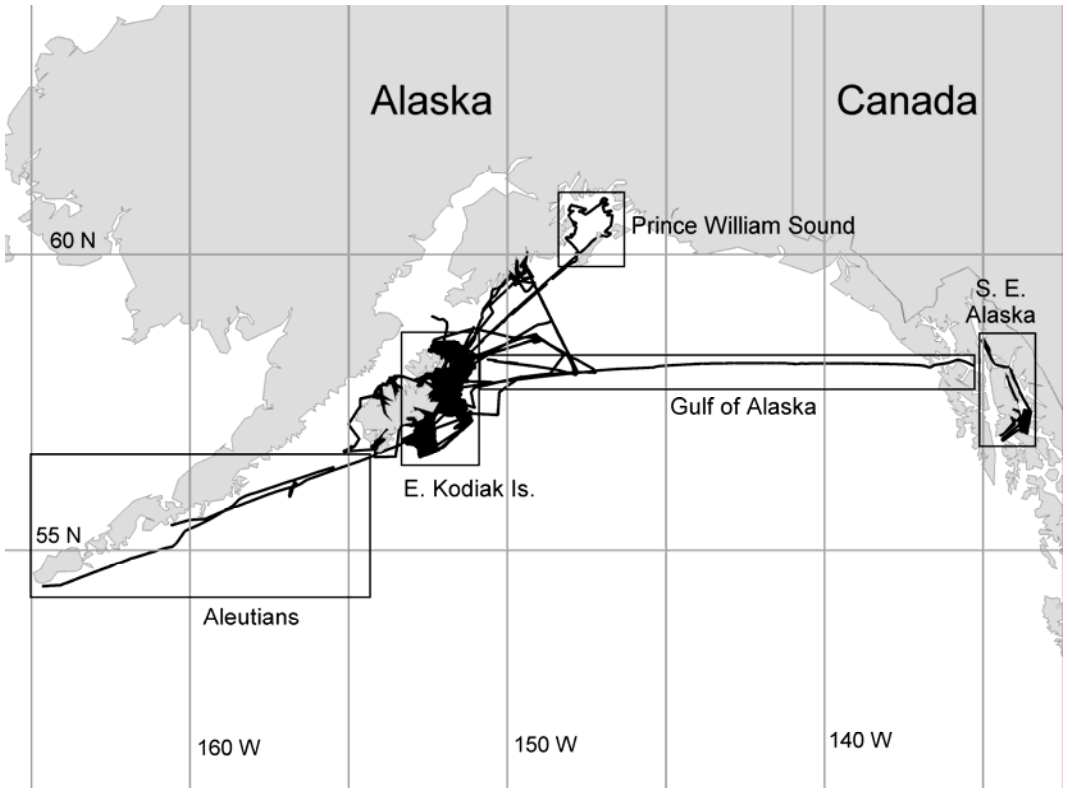

Fig. 13. 2002 Flight tracks from the Gulf of Alaska, along with the 5 regions used in the analysis.

While most of this work was near Kodiak Island, several flights were made to other regions, and it is interesting to compare the statistics by region. The results from these regions, all flown during the day, are summarized in Table 2. The fewest thin layers were observed in the waters very close to shore around Kodiak Island and in Southeast Alaska. For the waters around Kodiak Island, flow around the complex topography is likely to inhibit the formation of strong, persistent gradients. The most layers were observed in Prince William Sound and across the Gulf of Alaska; these were also the regions with the greatest average depth. The weakest layers were observed across the Gulf of Alaska. The strongest were in S.E. Alaska and in Prince William Sound; both of these areas are enclosed waters with large fresh-water influx, and might be expected to have strong density gradients.

Table 2. Results by region from 2002 data in Gulf of Alaska.

Region	Fraction	Depth	Thickness	Strength
Aleutians	0.055	4.6 m	2.3 m	1.6×10^{-5} m^{-1} sr^{-1}
E. Kodiak Is.	0.025	5.1 m	2.2 m	2.7×10^{-5} m^{-1} sr^{-1}
Prince William Sound	0.098	6.3 m	2.1 m	3.0×10^{-5} m^{-1} sr^{-1}
Gulf of Alaska	0.066	7.7 m	2.2 m	7.7×10^{-6} m^{-1} sr^{-1}
S.E. Alaska	0.031	4.7 m	2.0 m	4.5×10^{-5} m^{-1} sr^{-1}

For these flights, CTD casts were made in the area close to shore (within 100 km) to the SE of Kodiak Island. These will be compared with lidar data taken between August 11 and September 1, again within a 20 km radius of the cast. The delay between the lidar data and the CTD cast in this case is generally greater than in the NE Pacific, and can be as long as 2 weeks. Of 52 casts, 32 showed clear mixed layers. The range of values of the mixed layer depth was between 5 and 18 m, with an average value of about 10 m. The average density difference between surface and 50 m was 0.80, significantly less than in the previously described region. The average water depth at the cast locations was only about 118 m, with a weak correlation (R = 0.27) between water depth and mixed layer depth.

The average of the thin layer depth around the CTD casts was only about half of the mixed layer depth measured by the CTD, 4.6 m during the day and 5.2 m at night. The reasons for this discrepancy seem to be that the layers in this region have a large variation in depth, but only the shallower portions of the layers satisfy our criteria to be called thin. An example (Figure 14) shows a layer that varies in depth from about 3 m to about 15 m over a 2000 m section of the flight track. The only portion of this layer that was counted as thin, near the center of the figure, is at a depth of about 3.6 m. These data were taken during the day on August 16. The mixed layer depth from this cast was measured to be about 15 m on August 21. Note from the figure that the layer extends down to 15 m within a few hundred m of the position where the depth is 4 m.

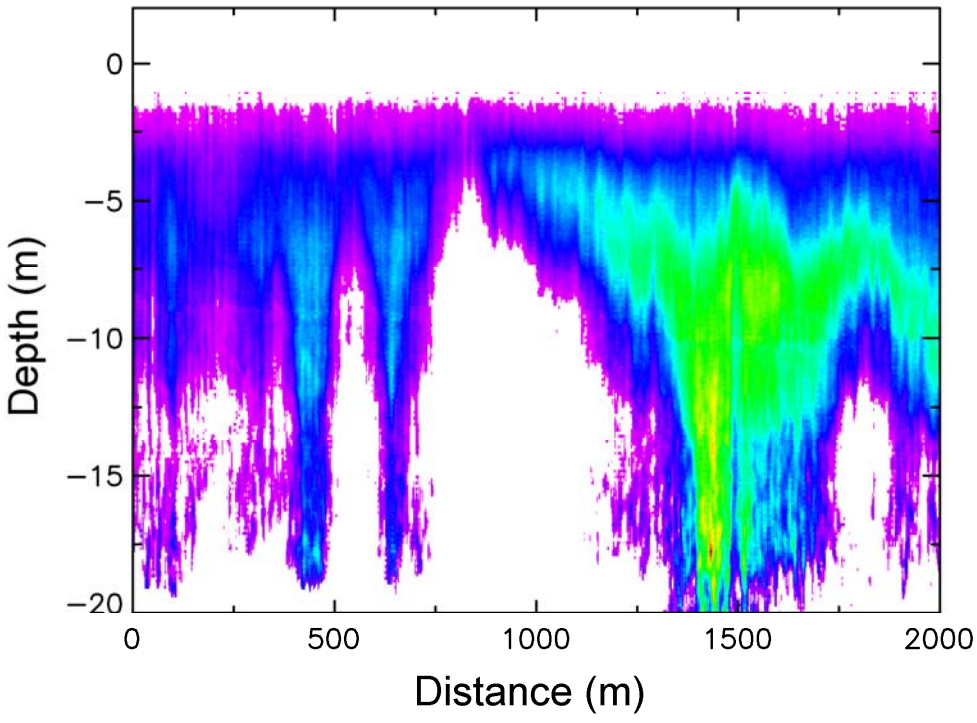

Fig 14. Vertical slice of lidar data near Kodiak Island.

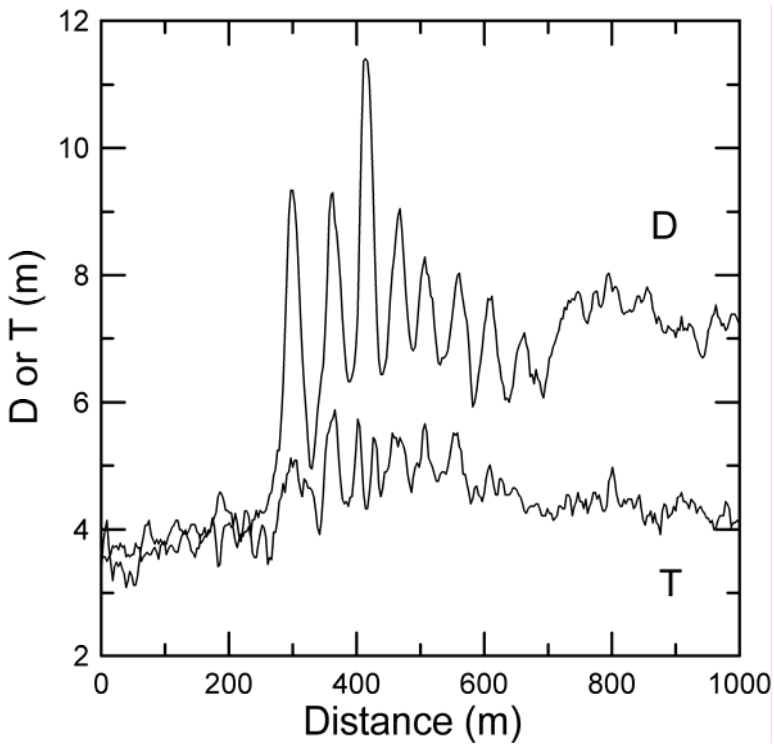

Fig. 15. Plot of depth D and thickness T of layer displaced by strong internal wave in Gulf of Alaska.

In the more open waters of the Gulf of Alaska, we observed a layer that spanned almost the entire Gulf (Churnside and Ostrovsky, 2004), although only portions of it satisfied our criteria for thin layers. This layer had more of the characteristic of a distinct layer with similar scattering strength above and below. Churnside and Ostrovsky described a strong internal wave propagating on this layer well away from the continental shelf. The depth of the layer changed from about 3.5 m before the wave passage to a little more than 7 m after the passage, with a maximum excursion to a depth of almost 12 m. The lidar image of this wave was presented in the reference, and will not be repeated hear. A plot of the depth of the maximum lidar return and the thickness of the layer (Figure 15) shows that the layer is 3.5 to 4 m thick before and after the internal wave passage. Within the wave, it gets somewhat thicker, with the thickest portions generally corresponding to the wave troughs.

3.3. Gulf of Alaska, 2001

Flights were also made in the Gulf of Alaska, including the region around Kodiak Island, between July 20 and September 10, 2001 (Figure 16). In all, about 8000 km were flown during daytime and 5000 km at night. Thin layers were observed in 1.5% of the daytime data and 0.19% of the nighttime, less than in 2002. The average daytime depth of 5.6 m was somewhat less than in 2002, but the average nighttime depth of 6.5 m was a little greater. The average thickness was about the same – 2.2 m during the day and 2.0 m at night. Again, multiple thin layers were very rarely observed.

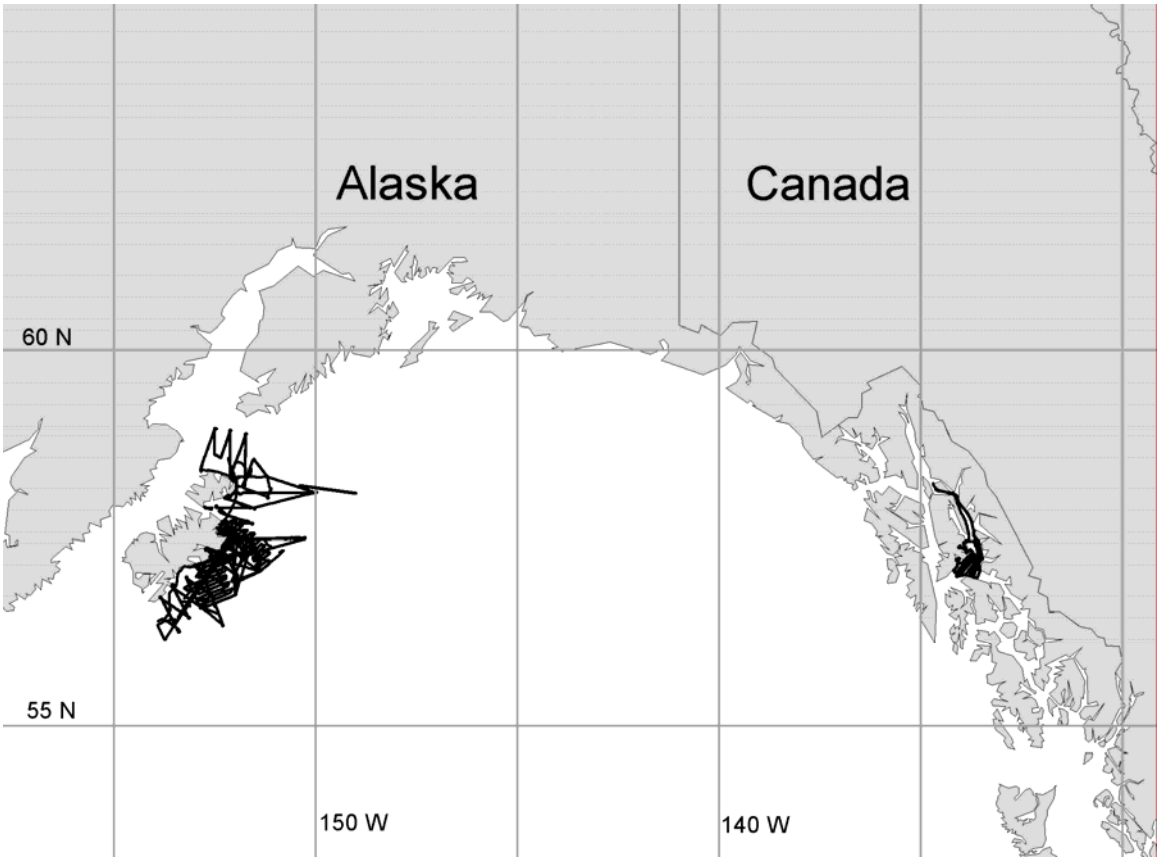

Fig. 16. 2001 flight tracks from the Gulf of Alaska.

As in 2002, there was not a good correspondence between layer depth and mixed layer depth. Forty seven CTD casts were made in the same near-shore region, and 32 of these showed clear mixed layers. The average depth of these layers was 13.5 m, somewhat deeper than in 2002. The average depth within 20 km of the CTD locations was 8.0 m during the day and 9.6 m at night.

Most of the time, the thin layers were similar to that in Figure 15, with a scattering layer of varying depth that extends to the surface. The thin parts of these were generally the lower edge of these at points where they were closest to the surface, and these were generally above the measured mixed layer depth.

In some cases, the measured mixed layer was above the observed layers. Figure 17 shows a segment of a thin layer at a depth of about 20 m, observed on August 13. The CTD casts in this area were made on August 26. Three density profiles show a large degree of variability in mixed layer depth (8, 13, and 17 m) over a short time span (just under 1.5 hours) and in a small area (just over 11 km). If we try to restrict the distance and time lag between the lidar observations and CTD casts to remove some of the effects of this variability, we do not end up with enough observations for a valid comparison.

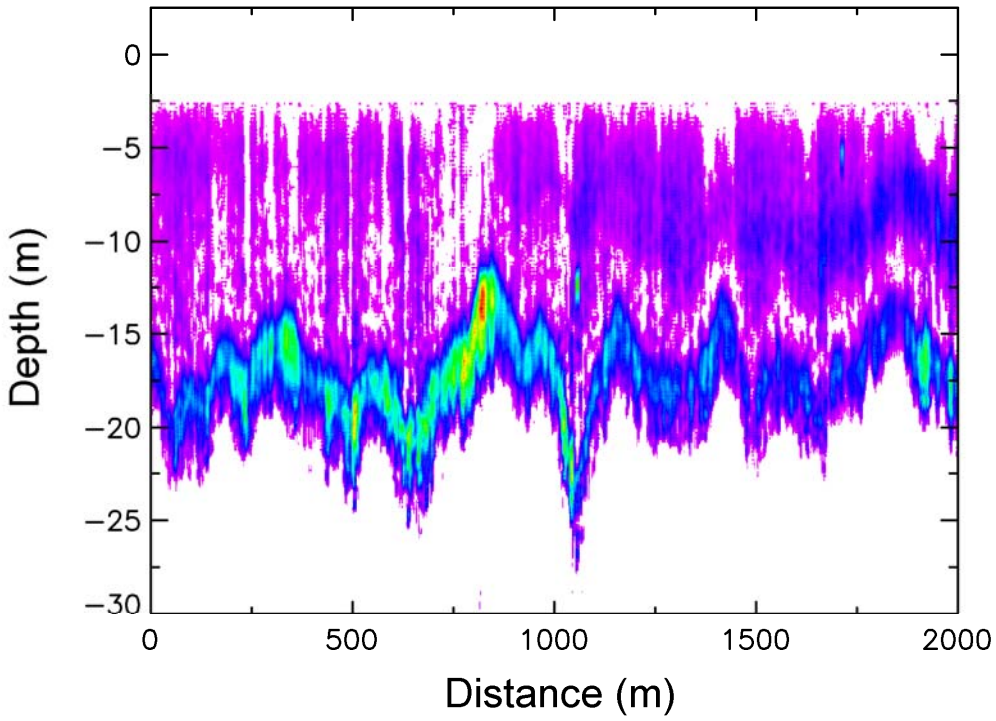

Fig. 17. Vertical slice of lidar data showing layer at a depth of 15 - 20 m.

A storm came through the area between August 18 and 23, and it is interesting to compare the situation around Kodiak Island before and after this storm. The CTD data show a deepening of the mixed layer, from an average value of 12 m before the storm to 15 m afterwards. The lidar data show significantly more thin layers before the storm than after – from 1.8 % to 0.31 % during the day and 0.22 % to 0.04 % at night. The depth of the observed layers actually decreases – from 5.8 m to 4.8 m during the day and 6.7 m to 4.0 m at night.

Fewer thin layers were observed in the S.E. Alaska region in 2001 than in 2002 – 1.4 % for the 2 daytime flights compared with 3.1 % during the day in 2002. The layers themselves were very similar, with an average depth of 4.5 m and an average thickness of 1.8 m.

3.4. Gulf of Alaska, 2003

In the summer of 2003, we flew another series of flights in the Gulf of Alaska, all during the daytime. As the flight tracks in Figure 18a show, these were not concentrated around Kodiak Island, but extended over a broad area with data collected along 6500 km. Overall, 5.1 % of the data contained thin layers, with an average depth of 10.8 m and an average thickness of 2.2 m. The prevalence of thin layers is similar to what we saw in

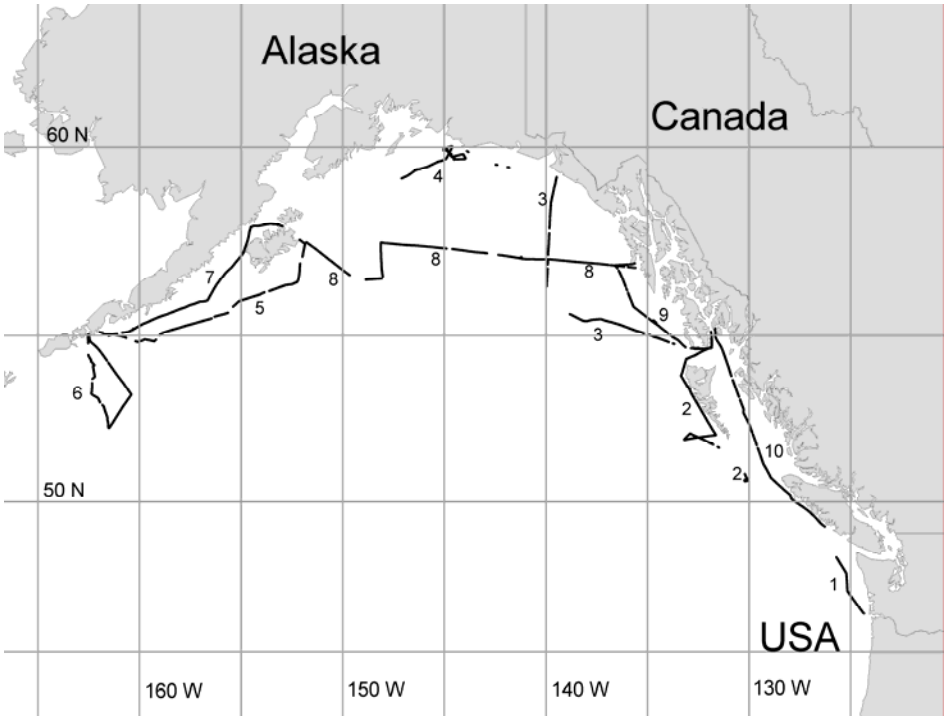

Fig. 18a. Map of 2003 Gulf of Alaska flight tracks, labeled by flight number. Tracks show only locations of data collection, not full flight tracks.

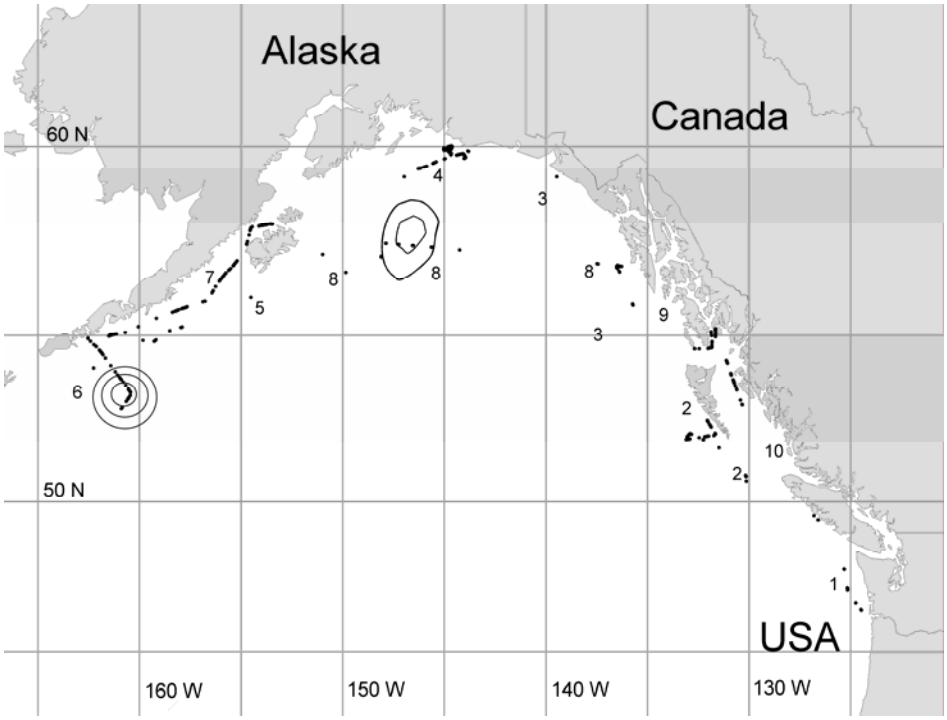

Fig. 18b. Map of thin layer locations within the flight tracks of Fig. 18a. Concentric lines represent sea surface height anomaly contours of 0.1, 0.2, and 0.3 m from the outside in.

previous years in the Gulf of Alaska, but the average depth is significantly greater. Because these flights cover such a large area, it is instructive to separate the data by individual flight, labeled by number in Figure 18. The actual distribution of observed thin layers is presented in Figure 18b. The measured parameters, summarized in Table 3, show a large variation.

Table 3. Results by flight from 2003 data in Gulf of Alaska.

Flight Number	Fraction	Depth	Thickness	Strength
1	0.031	5.3 m	1.4 m	1.5×10^{-6} m^{-1} sr^{-1}
2	0.058	16.0 m	2.2 m	2.3×10^{-6} m^{-1} sr^{-1}
3	0.009	7.1 m	2.1 m	4.6×10^{-6} m^{-1} sr^{-1}
4	0.194	9.1 m	2.1 m	6.9×10^{-6} m^{-1} sr^{-1}
5	0.004	13.5 m	1.7 m	2.9×10^{-6} m^{-1} sr^{-1}
6	0.031	15.8 m	2.1 m	2.5×10^{-6} m^{-1} sr^{-1}
7	0.140	9.3 m	2.3 m	5.7×10^{-6} m^{-1} sr^{-1}
8	0.020	15.6 m	2.2 m	1.0×10^{-6} m^{-1} sr^{-1}
9	0.015	14.2 m	2.3 m	9.0×10^{-7} m^{-1} sr^{-1}
10	0.038	6.7 m	2.3 m	5.8×10^{-6} m^{-1} sr^{-1}

The first flight, off the coast of Washington State, observed layers that were similar to those in the same area just previously as part of the program denoted by NW Pacific Ocean. For example, we note that this flight track went near three of the CTD casts from that program, the one closest to shore on the 46th parallel, and the next one out on both the 47th and 48th. The average layer depth observed previously near these three casts was 6.6 m, which is similar to the average depth of 5.3 m that was observed in this flight.

Most of the second flight was along the west coast of the Queen Charlotte Islands, British Columbia and into Ketchikan, Alaska. A few relatively shallow layers were observed inside the islands of SE Alaska, but most were outside the Queen Charlotte Islands and to the south, where the flight track was farther off shore. None were observed along the northern west coast of the islands, where the flight track was closer to shore. The layers off the southwestern Queen Charlotte Islands were some of the deepest observed. Figure 19 shows a typical example of a layer in this region. It is thin, according to our criteria, from about 500 m to about 3500 m in the figure. After that it becomes thicker, and a very diffuse layer extends up toward the surface.

The next two flights, in the northern part of the gulf, were very different. Almost no thin layers were observed in the third flight, which extended out in the eastern part of the Gulf of Alaska. The few that were observed were close to shore at either the beginning of the flight near Ketchikan or the end near Yakatat. By contrast, the fourth flight, closer to shore along the northernmost part of the gulf, had a much higher number of thin layers. These tended to be slightly deeper and stronger.

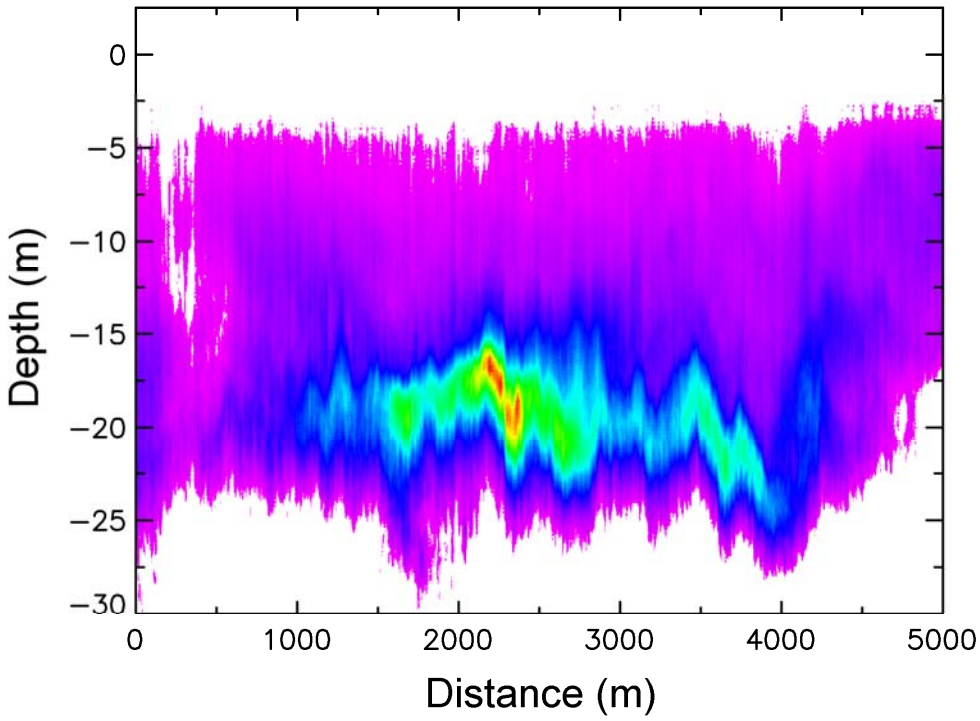

Fig. 19. Vertical slice of lidar data off the southwestern Queen Charlotte Islands.

A similar pattern emerges in data from flights 5 and 7, which are from Kodiak to Cold Bay and back. Very few layers were observed in the flight to Cold Bay, which was farther off shore. Many more were observed closer to shore in the return flight. In this region, the near-shore layers were closer to the surface than those farther offshore, although they were slightly stronger, as in the northern Gulf.

Flight 6, south of Cold Bay, shows more layers offshore than seen in other regions. This is interesting, because the data sample the center and western edge of a warm-core eddy identified in images of sea-surface height, sea-surface temperature, and ocean color from satellite instruments. The location of the eddy, as measured by sea-surface height anomaly on the day after flight 6 (31 July 2003), is identified in Figure 18b. The region near the center of the eddy contains a large layer with numerous regions that satisfy our criteria to be designated thin. The region along the western edge of the eddy shows no such layer.

Flight number 8, across the gulf, also passed through the center of a warm-core eddy, which extended from about 144 W to 148 W. This flight was made the day after the 31 July altimeter measurement, and the contours of surface-height anomaly from that measurement are also plotted in Figure 18b. Most of the thin layers in the center of the gulf along this flight track were associated with that eddy, and were very similar in

appearance and depth to those associated with the eddy south of Cold Bay. On this flight, we did not see a large layer extending across most of the gulf as we did just to the north in May 2002. There is another layer near the intersection of flights 8 and 9, which was observed in both flights. In fact, this region accounts for most of the detected layers in flight 9.

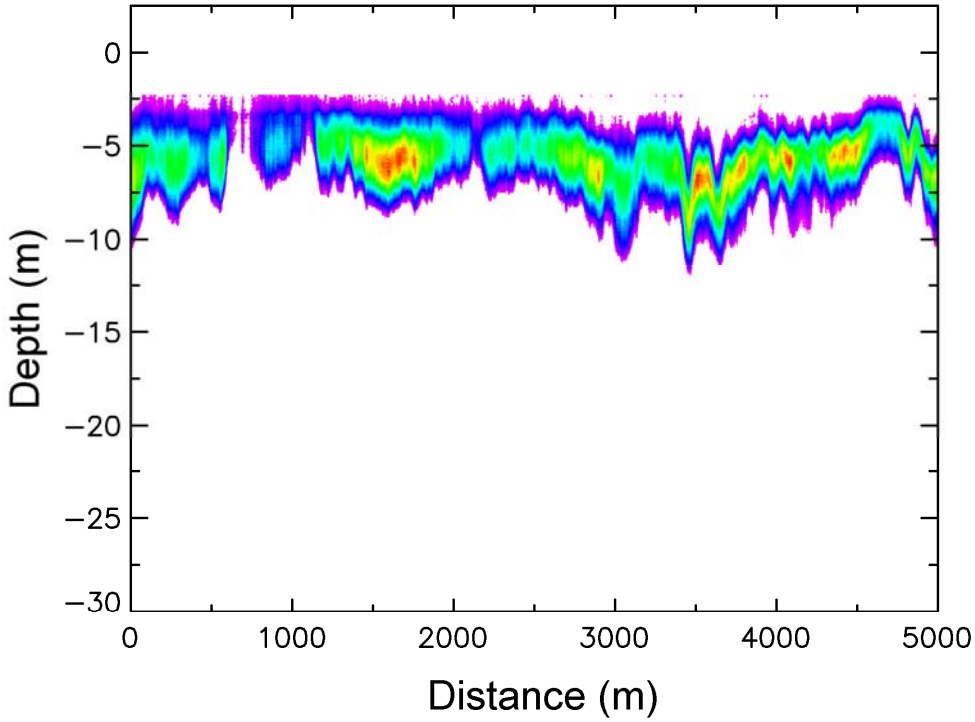

Fig. 20. Vertical slice of lidar data to the east of the Queen Charlotte Islands.

In the final flight, most of the observed layers were to the east of the Queen Charlotte Islands. These were generally stronger and closer to the surface than those observed to the west of the islands. As an example, compare the layer extending from a distance of about 400 m to about 4500 m in Figure 20 with a corresponding layer from the other side of the islands. The two layers look very similar, except that the depth is significantly different.

3.5. Norwegian Sea, 2002

In 2002, about 8000 km (Figure 21) were flown during the day over the Norwegian Sea. During most of the period, the weather was determined by weak low pressure to the west and generally moderate winds. Water density gradients were also generally moderate, with an average difference between the value of the density σ_θ at a depth of 50 m and at the surface of 1.7 kg m^{-3}. Almost all values were between 1 and 2

kg m^{-3}, except near the southern coast of Norway. There, fresher water at the surface produced greater differences.

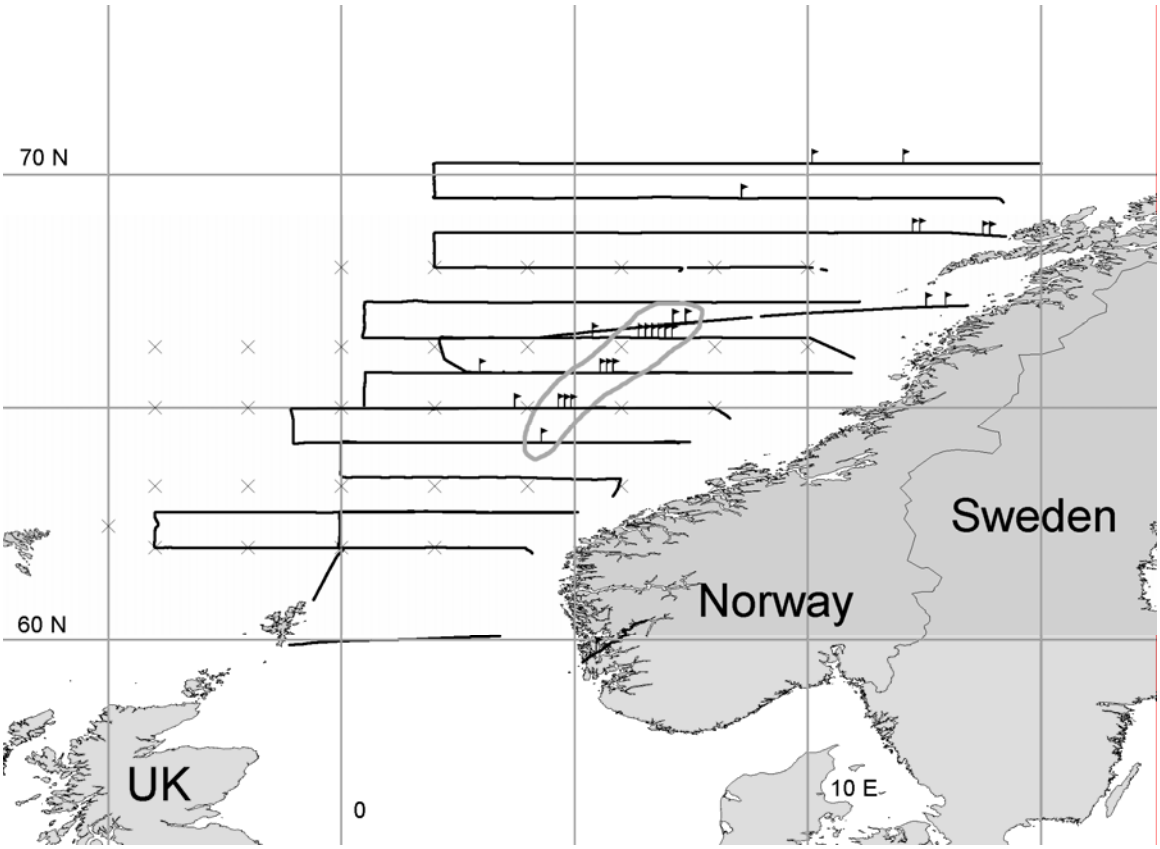

Fig. 21. 2002 flight tracks off the coast of Norway. Flags show locations of observed thin layers; the grey line encloses the region with the greatest density of layers.

The fraction of thin layers in these data is much lower – 0.22%. The average depth was 11.2 m, and the average thickness was 2.1 m. The thin layers that were observed (also in Figure 21) were 1) a broad band (enclosed within a grey line in the figure) roughly parallel to the coastline from about 64 N to about 67 N, 2) closer to the coast around the Lofoten Islands, and 3) in the fjord south of Bergen (just south of 60 N and east of 5 E in the figure).

The type of comparison of mixed layer depth and thin layer depth that was done in other areas is not possible in this area. CTD casts were made between 62 N and 68 N, but only one, on 65 N, was within 20 km of observed thin layers. The mixed layer depth at this cast was estimated to be at about 16 m. The three thin layers closest to this were at depths of 6.6 m, 13.6 m, and 17.1 m. These layers were not as strong or as well organized as those within the region outlined by the grey line in Figure 21. That is, they do not show up clearly in the unprocessed data.

From the data within the grey line in Figure 21, it appears that this area may contain a very large layer with numerous thin portions. Figure 22 is a typical example of layers in this region. They include layers going right to the surface, and double layers, and layers down to 20 m. The shaded region lies roughly along the eastern edge of the 1400 m deep Vøring Plateau (Nilsen and Falck, 2005), which may have an effect on layer formation through its effects on the eastern branch of the Norwegian Atlantic Current.

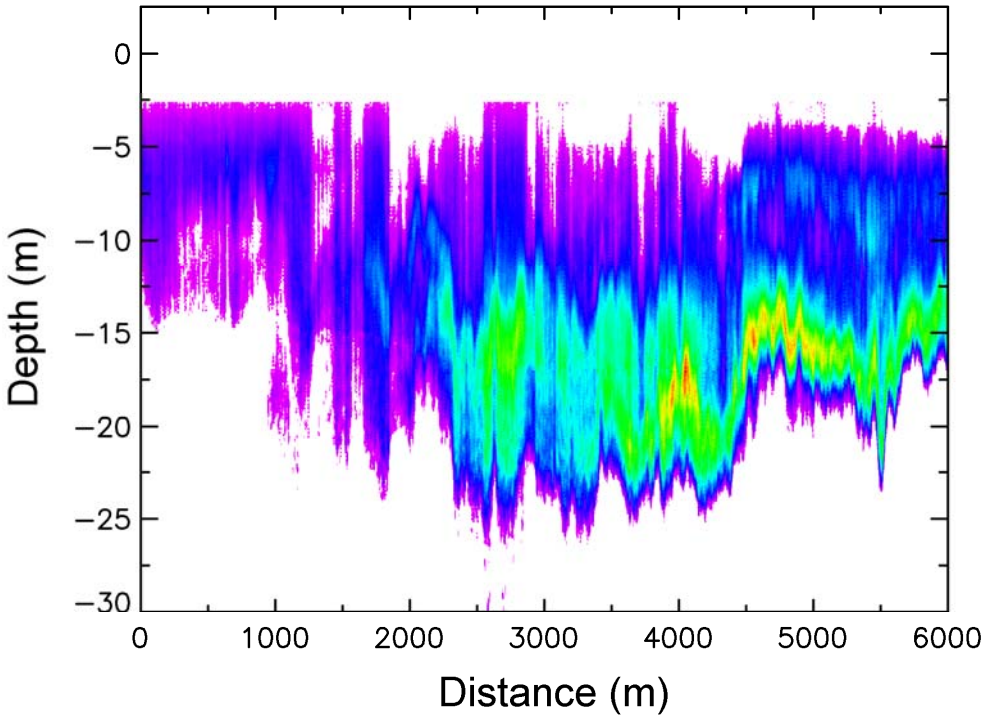

Fig. 22. Vertical slice of lidar data from region within grey line in Fig. 21.

The layers closer to shore are somewhat different. Figure 23 shows the westernmost thin layer on the third transect from the top. At 1000 m from the left side of the plot, there is a layer at a depth of about 20 m that is oscillating with a wavelength of about 165 m. This portion did not qualify as a thin layer. Between 2000 m and 4000 m, this layer gets shallower and thinner, and about 30 % of the layer from 3000 m to the end of this segment is thin. At 5000 m the layer depth is about 6.5 m, and the wavelength of the oscillation is about 68 m. While we do not have CTD information in this area, the characteristics of this layer are consistent with a deeper and weaker pycnocline at 1000 m and a shallower and stronger one at 5000 m. Using the expression for a 2-layer system, we can estimate the relative frequencies of the 2 waves if the densities of the top and bottom layers are the same for both cases. In this case, the deeper wave would have a frequency of about 0.7 times that of the shallower wave.

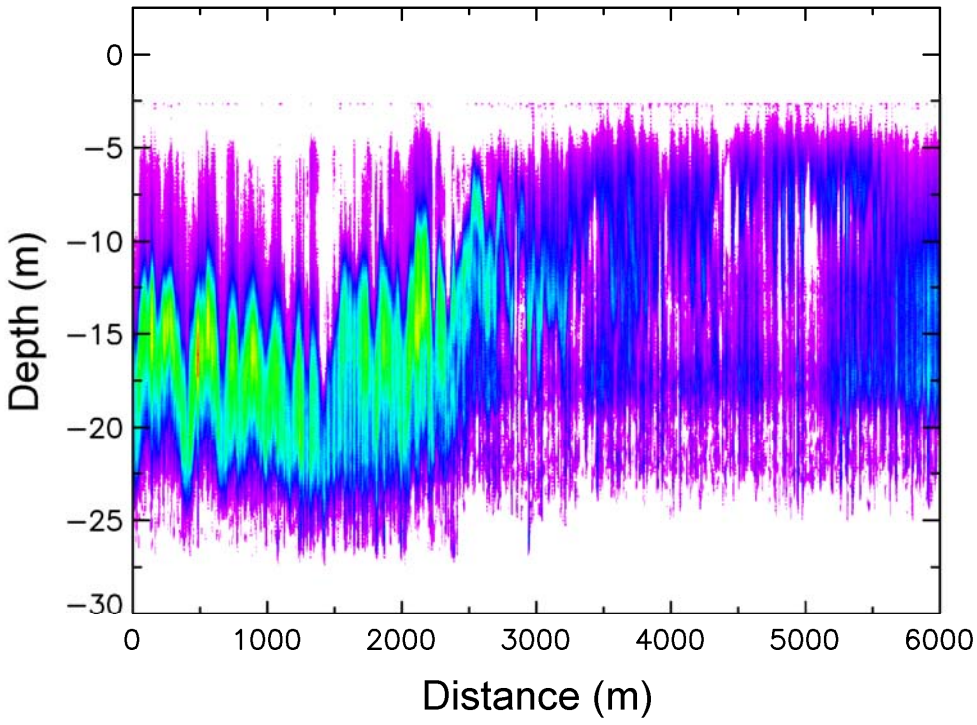

Fig. 23. Vertical slice of lidar data from the northern portion of the survey area in Fig. 21.

3.6. Atlantic, near Iberian Peninsula, 1998

In 1998, we flew almost 5000 km off the west coast of Spain and Portugal and in the Bay of Biscay north of Spain (Figure 24). About 24% of the total was flown at night. During the daytime, we observed thin layers in about 1.4 % of the area, and about 3.8 % in the night flights. The average depth was about 8.1 m during the day and about 8.9 m at night. The average thickness was less than observed elsewhere, 1.7 m during the day and

Table 4. Results by region from 1998 data near Iberian Peninsula.

Region	Conditions	Fraction	Depth	Thickness
Galicia	daytime	0		
Galicia	nighttime	0.034	3.8 m	1.7 m
Portugal	daytime	0.038	8.2 m	1.7 m
Bay of Biscay	daytime, before storm	0.004	6.6 m	2.3 m
Bay of Biscay	nighttime, before storm	0.041	11.8 m	1.9 m
Bay of Biscay	after storm	0		

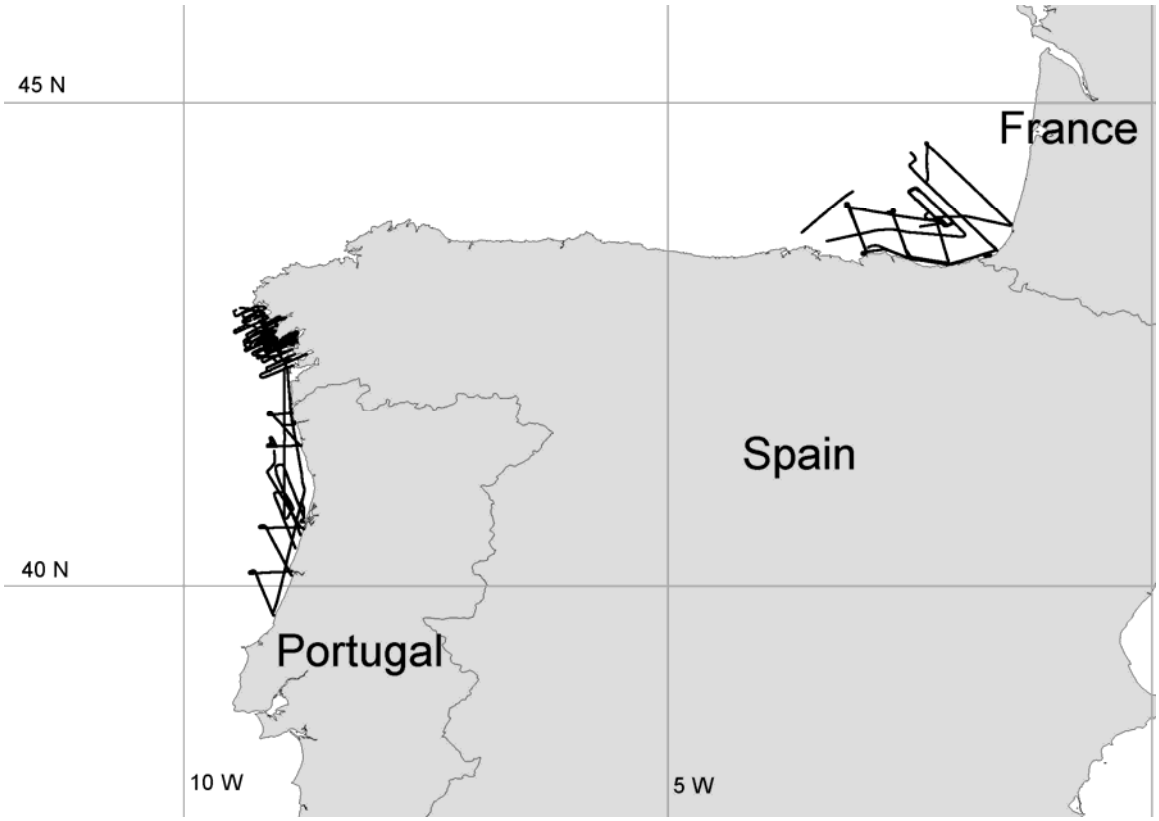

Fig. 24. 1998 flight tracks near the Iberian Peninsula.

1.8 m at night. As in other areas, there are some significant differences in different parts of the area (Table 4).

The flights off the northwest coast of Spain were largely within the inlets along the coast. No thin layers were observed in this region during the day. Only at night did thin layers appear, covering 3.4 % of the flight track at an average depth of 3.8 m and an average thickness of 1.7 m. Also, these layers did not exhibit the wave structures that occur in almost all of the layers described up to this point; they seem to be very nearly parallel to the surface.

Almost all of the observed daytime layers were off the coast of Portugal. Only daytime flights were made in this area, but layers were observed in 3.8 % of the sampled region. The average depth was 8.2 m, and the average thickness was 1.7 m. These layers are very strong (Figure 25) compared with other layers observed during this experiment. Estimates of volume backscatter coefficient are not available, however, as the lidar was not calibrated. Note also that these layers show the waviness that is a feature of layers in most areas.

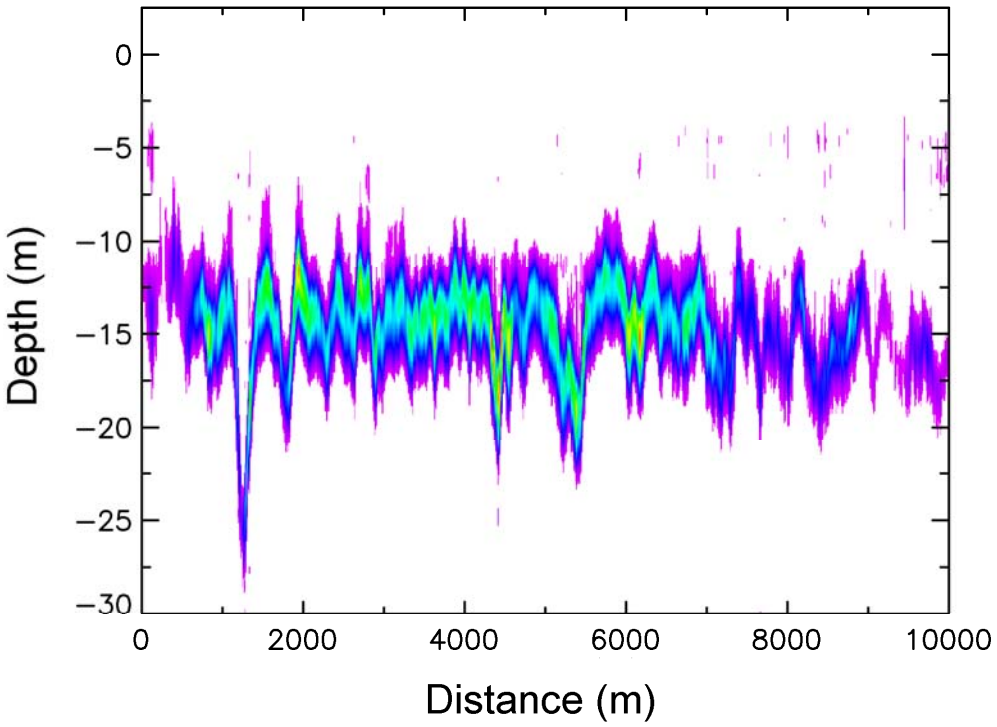

Fig. 25. Vertical slice of lidar data showing a strong layer off the coast of Portugal.

Available hydrographic data (Rosa, et al, 1998) in this region are consistent with the hypothesis that the layers are at the bottom of the mixed layer. Three east-west transects were made between September 5 and 7, just after the flights on August 31 and September 2. The 18.5° isotherm is generally considered to be the bottom of the mixed layer in this area (Rosa, et al, 1998), and this depth was used for 15 of the casts. For 4 additional casts in the northwest part of the surveyed area, this isotherm was above the minimum reported depth of 5 m. In these cases, we used the 18° depth taken from the data or from an extrapolation of the data. The region covered, between 40.55 N and 41.18 N, was a small part of the aerial survey region, and there was no significant correlation between mixed layer depth and thin layer depth. This is probably partly due to a difference in meteorological conditions. During the flights, winds were southerly, while during the hydrographic cruise, they were more westerly, leading to more upwelling. This upwelling condition also existed for most of the month of August before the flights.

While weather differences probably affected the small-scale distribution of the mixed layer depth, the overall range of mixed layer depth and of thin layer depth within the hydrographic survey area are similar. The inferred mixed layer depth had an average value of 8.7 m, with a range of values from 3.8 m to 16.8 m. The observed thin layers had an average depth of 7.4 m, with a range of values from 3.5 m to 14.6 m.

The flights over the Bay of Biscay were separated by a 6 day gap, from September 9 to 15, by a large storm that moved through the area. Before the storm, layers were observed mostly at night and mostly close to the coast. During the day, only 0.4 % of the flight track contained thin layers. These had an average depth of 6.6 m and an average thickness of 2.3 m. At night, the fraction was much higher (4.1 %), the depth greater (11.8 m), and the thickness less (1.9 m). Overall, 81 % of the extent of the thin layers was within 10 km of the coast, including all of those observed during the day. No layers were observed in the two daytime flights after the storm. There is no evidence that this was an effect of the storm; these flights did not include the areas close to shore.

3.7. California Bight, 1997

The first fish lidar tests were made off the coast of Southern California (Figure 26) between March 30 and April 21 1997. We flew a little over 6000 km during daytime and a little less than this amount at night. During most of this period, the area was subject to strong NW winds, leading to strong upwelling (Figure 27). Winds as high as 15 m s^{-1} were recorded during the April 1997 California Cooperative Fisheries Investigation (CalCOFI) cruise (http://www.calcofi.org). Hydrographic data from the same cruise (http://www.calcofi.org) show little evidence of stratification. The reported profiles do not have enough vertical resolution to identify narrow regions of strong vertical density gradient near the surface, but some indication can be obtained by looking

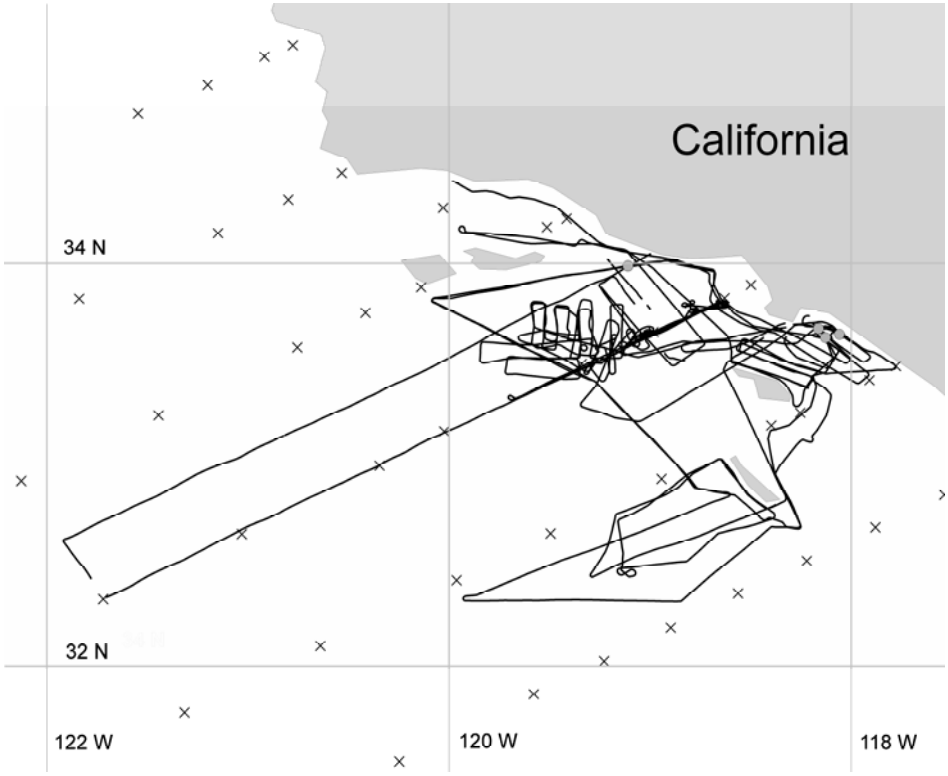

Fig. 26. Flight tracks for 1997 flights near Southern California. Crosses mark CTD casts and grey circles mark locations of layers. An additional 2 layers were observed north of the area in the map during the transit from Sacramento to the survey area.

at the total difference between the value of σ_θ at a depth of 50 m and the value at the surface. The average over all of the CalCOFI stations was only 0.38 kg m^{-3}. The greatest value was 1.18 kg m^{-3}. Values for stations on the outer half of the lines were generally very small (<0.1 kg m^{-3}).

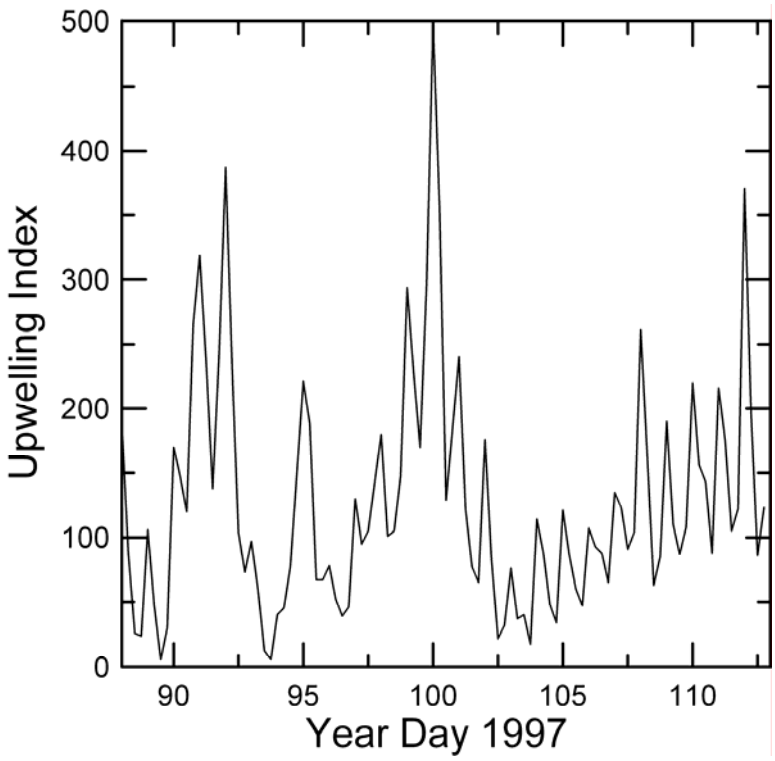

Fig. 27. Upwelling index (m^3 s^{-1} per 100 m of coastline) at 33 N 119 W during the period of the California flights. Data from http://las/pfeg.noaa.gov.

Only a handful of layers were observed – 0.05 % of the track during the day and 0.02 % at night. All were within 10 km of the coastline. The average depth was 10.4 m during the day and 6.3 m at night; average thickness was 1.9 m during the day and 2.2 m at night. All of these layers were observed before the large upwelling event during a relatively quiet period around days 96 and 97 in Figure 27.

CalCOFI data can be used to estimate mixed layer depth. Vertical resolution is rather poor for our purposes, so we estimate mixed layer depth using a linear extrapolation of σ_θ. The southernmost 3 layers in the map have depths of 7.3 m, 8.0 m, and 10.7 m. The mixed layer depths estimated from the closest two stations to the SE of these layers were 7.5 m (Station 90.30) and 17 m (Station 90.28). The density gradients across the top 50 m at these two sites were among the largest measured at sites within the area covered by the flights at 0.88 and 1.13 kg m^{-3}, respectively. These casts were made within 4 days of the LIDAR observations. The next layer to the northwest had a depth of 5.2 m. The two closest near-shore stations in this case were those to the NW. These had estimated mixed layer depths of 2.3 m (Station 83.40) and 8.0 m (Station 83.42), but

these casts were made after the high-wind event. The first cast did not reach 50 m in depth, and the second had an overall gradient of 0.36 kg m^{-3}..

4. Conclusions

An airborne LIDAR is capable of measuring thin optical scattering layers in the upper ocean. Over 2000 km of optically thin layers were identified in about 80000 km of flight tracks. The structure of these layers varied significantly from region to region, especially between near-shore and off-shore layers. Spatial structures included multiple layers, sharp changes in depth, and internal-wave-like perturbations. Because of these structures, detailed comparison with CTD measurements requires that the LIDAR measurement and the CTD cast be close together in both space and time. In coastal regions with strong internal-wave fields, the differences should be much less than the wavelength and period of those waves.

The most thin layers were identified in regions where there were large differences in density, especially where there was a significant amount of fresh water inflow, like the Columbia River Plume and Prince William Sound. Few layer were detected during high-wind events, whether they were associated with strong upwelling (as in California) or not (as in Kodiak). In general, thin layers were more prevalent over the continental shelf than farther off shore. One notable exception to this rule was the detection of thin layers within warm-core eddies in the Gulf of Alaska.

While the LIDAR was successful in identifying thin layers according to the definition used here, the current configuration is not capable of resolving layers that are much thinner than the 3 m criterion. Two modifications would allow resolution of layers down to 10 – 20 cm. The first is to shorten the laser pulse length from the current value of about 12 ns to about 1 ns. This provides a resolution in water of about 10 cm. The second is to narrow the beam divergence and the field of view of the receiver. Narrowing the field of view to about 1.7 mrad will produce a 10 cm depth difference across the beam for a 15˚ incidence angle. An incidence angle closer to nadir will allow a wider beam to get the same effect.

Another improvement for thin layer surveys would be the addition of a second receiver channel to obtain the depolarization ratio. This would aid in identification of the type of scattering particles present. This would be particularly interesting for scattering layers right at the surface, since bubbles would very nearly preserve polarization, while particles with non-spherical geometries, like plankton, would tend to depolarize the scattered light.

Acknowledgments

This analysis was partially supported by the Office of Naval Research. 2003 CTD data from the NE pacific were provided by Dave Griffith of the NOAA Southwest Fisheries Science Center. 2001 and 2002 CTD data from the area around Kodiak Island were provided by Mike Guttormsen of the NOAA Alaska Fisheries Science Center. CTD data from the Norwegian Sea were provided by Eirik Tenningen of the Norwegian Institute of Marine Research.

References

Alldredge, A.L., T.J. Cowles, S. MacIntyre, J.E.B. Rines, P.L. Donaghay, C.F. Greenlaw, D.V. Holliday, M.M. Dekshenieks, J.M. Sullivan, J.R.V. Zaneveld (2002), Occurrence and mechanisms of formation of a dramatic thin layer of marine snow in a shallow Pacific fjord, *Mar. Ecol. Prog. Ser. 233*, 1-12.

ANSI, (1993), *Safe Use of Lasers, Standard Z-136.1,* (American National Standards Institute, New York.

Churnside, J. H., J. J. Wilson, and V. V. Tatarskii, Lidar profiles of fish schools, *Appl. Opt. 36*, 6011-6020 (1997).

Churnside, J. H., J. J. Wilson, and V. V. Tatarskii (2001), Airborne Lidar for Fisheries Applications, *Opt. Eng. 40*, 406-414.

Churnside, J. H., D. A. Demer, and B. Mahmoudi (2003), A Comparison of Lidar and Echosounder Measurements of Fish Schools in the Gulf of Mexico, *ICES J. Mar. Sci. 60*, 147–154.

Churnside, J. H. and L. A. Ostrovsky (2004), Lidar observation of a strongly nonlinear internal wave train in the Gulf of Alaska, *Int. J. Remote Sens. 26*, 167-177.

Cowles, T. J., R. A. Desiderio, and M-E Carr (1998), Small-scale planktonic structure: persistence and trophic consequences, *Oceanography 11*, 4-9.

Dekshenieks, M. M., P. L. Donaghay, J. M. Sullivan, J. E. B. Rines, T. R. Osborn, and M. S. Twadowski (2001), Temporal and spatial occurrence of thin phytoplankton layers in relation to physical processes, *Mar. Ecol. Prog. Ser. 223*, 61-71.

Gordon, H. R. (1982), Interpretation of airborne oceanic lidar: effects of multiple scattering, *Appl. Opt. 21*, 2996-3001.

Hanson, A. K. Jr. and P. L. Donaghay (1998), Micro- to fine-scale chemical gradients and layers in stratified coastal waters, *Oceanography 11*, 10-17.

Hoge, F. E., C. W. Wright, W. B. Krabill, R. R. Buntzen, G. D. Gilbert, R. N. Swift, J. K. Yungel, and R. E. Berry (1988), Airborne lidar detection of subsurface oceanic scattering layers, *Appl. Opt. 27*, 3969-3977.

Holliday, D.V., P.L. Donaghay, C.F. Greenlaw, D. E. McGehee, M.M. McManus, J.M. Sullivan and J.L. Miksis (2003), Advances in defining fine- and micro-scale pattern in marine plankton, *Aquatic Living Resources 16*, 131-136.

Holliday, D. V., R. E. Pieper, C. F. Greenlaw, and J. K. Dawson (1998), Acoustic sensing of small-scale vertical structures in zooplankton assemblages, *Oceanography 11*, 18-23.

Lewis, G. D., D. L. Jordan, and P. J. Roberts (1999), Backscattering target detection in a turbid medium by polarization discrimination, *Appl. Opt. 38*, 3937-3944.

McManus, M.A., A.L. Alldredge, A.H. Barnard, E. Boss, J.F. Case, T.J. Cowles, P.L. Donaghay, L.B. Eisner, D.J. Gifford, C.F. Greenlaw, C.M. Herren, D.V. Holliday, D. Johnson, S. MacIntyre, D.M. McGehee, T.R. Osborn, M.J. Perry, R.E. Pieper, J.E.B. Rines, D.C. Smith, J.M. Sullivan, M.K. Talbot, M.S. Twardowski, A. Weidemann and J.R. Zaneveld (2003), Characteristics, Distribution and Persistence of Thin Layers Over a 48-Hour Period, *Mar. Ecol. Prog. Ser. 261*, 1-19.

Nilsen, J. E. Ø. And E. Falck (2005), Variations of mixed layer properties in the Norwegian Sea for the period 1948-1999, submitted to *Progress in Oceanography*.

Petrenko, A. A., J. R. V. Zaneveld, W. S. Pegau, A. H. Barnard, and C. D. Mobley (1998), Effects of a thin layer on reflectance and remote-sensing reflectance, *Oceanography 11*, 48-50.

Pieper, R. E. and D. V. Holliday (1984), Acoustic measurements of zooplankton distributions in the sea, *J. Cons. Int. Explor. Mer. 41*, 226-238.

Rose, T., A. Peliz, and A. M. P. Santos (1998), Hydrographic survey in the central Iberian Atlantic coast in September 1998, in *JUVESU Report on Experimental Surveys for the Assessment of Juveniles,* Directorate General for Fisheries DG XIV, Commission of the European Communities, Brussels.

Stabeno, P. J., N. A. Bond, A. J. Hermann, N. B. Kachel, C. W. Mordy, and J. E. Overland (2004), Meteorology and oceanography of the Northern Gulf of Alaska, *Continental Shelf Res. 24*, 589-897, doi:10.1016/j.csr.2004.02.007.

Vasilkov, A. P., Y. A. Goldin, B. A. Gureev, F. E. Hoge, R. N. Swift, and C. W. Wright (2001), Airborne polarized lidar detection of scattering in the ocean, *Appl. Opt. 40*, 4353-4364.

Zaneveld, R. J. V. and W. S. Pegau (1998), A model for the reflectance of thin layers, fronts, and internal waves and its inversion, *Oceanography 11*, 44-47

Zorn, H. M., J. H. Churnside, and C. W. Oliver (2000), Laser Safety Thresholds for Cetaceans and Pinnipeds, *Marine Mammal Sci. 16*, 186-200.